Late Quaternary palaeoenvironment of northern Guatemala: evidence from deep drill cores and seismic stratigraphy of Lake Petén Itzá

Mueller, Andreas; Anselmetti, Flavio S.; Ariztegui, Daniel; Brenner, Mark; Hodell, David A.; Curtis, Jason H.; Escobar, Jaime; Gilli, Adrian; Grzesik, Dustin A.; Guilderson, Thomas P.; Kutterolf, Steffen; Plötze, Michael

Late Quaternary palaeoenvironment of northern Guatemala: evidence from deep drill cores and seismic stratigraphy of Lake Petén Itzá

ANDREAS D. MUELLER*, FLAVIO S. ANSELMETTI†, DANIEL ARIZTEGUI‡, MARK BRENNER§, DAVID A. HODELL¶, JASON H. CURTIS§, JAIME ESCOBAR§, ADRIAN GILLI*, DUSTIN A. GRZESIK§, THOMAS P. GUILDERSON**, STEFFEN KUTTEROLF†† and MICHAEL PLÖTZE‡‡

Geological Institute, Swiss Federal Institute of Technology ETH Zurich, 8092 Zurich, Switzerland (E-mail: andreas.mueller@erdw.ethz.ch)

†*Eawag (Swiss Federal Institute of Aquatic Science & Technology), Department of Surface Waters, 8600 Duebendorf, Switzerland*

‡*Section of Earth and Environmental Sciences, University of Geneva, 1205 Geneva, Switzerland*

§*Department of Geological Sciences and Land Use and Environmental Change Institute (LUECI), University of Florida, Gainesville, FL 32611, USA*

¶*Department of Earth Sciences, University of Cambridge, Cambridge CB2 3EQ, UK*

**Center for Accelerator Mass Spectrometry, Lawrence Livermore National Laboratory, Livermore, CA 94550, USA*

††*Leibniz Institute for Marine Sciences, IfM-Geomar, 24148 Kiel, Germany*

‡‡*ClayLab, Institute for Geotechnical Engineering, Geological Institute, Swiss Federal Institute of Technology ETH Zurich, 8093 Zurich, Switzerland*

Associate Editor – Chris Scholz

ABSTRACT

Long sediment cores were collected in spring 2006 from Lake Petén Itzá, northern Guatemala, in water depths ranging from 30 to 150 m, as part of an International Continental Scientific Drilling Program project. The sediment records from deep water consist mainly of alternating clay, gypsum and carbonate units and, in at least two drill sites, extend back >200 kyr. Most of the lithostratigraphic units are traceable throughout the basin along seismic reflections that serve as seismic stratigraphic boundaries and suggest that the lithostratigraphy can be used to infer regional palaeoenvironmental changes. A revised seismic stratigraphy was established on the basis of integrated lithological and seismic reflection data from the basin. From *ca* 200 to *ca* 85 ka, sediments are dominated by carbonate-clay silt, often interbedded with sandy turbidites, indicating a sediment regime dominated by detrital sedimentation in a relatively humid climate. At *ca* 85 ka, an exposure horizon consisting of gravels, coarse sand and terrestrial gastropods marks a lake lowstand or partial basin desiccation, indicating dry climate conditions. From *ca* 85 to *ca* 48 ka, transgressive carbonate-clay sediments, overlain by deep-water clays, suggest a lake level rise and subsequent stabilization at high stage. From *ca* 48 ka to present, the lithology is characterized by alternating clay and gypsum units. Gypsum deposition correlates with Heinrich Events (i.e. dry climate), whereas clay units coincide with more humid interstadials.

Keywords Guatemala, lake level changes, lake sediments, palaeoclimatology, Petén Itzá, seismic stratigraphy.

INTRODUCTION

Palaeoenvironmental studies in the lowlands of Petén, northern Guatemala (Fig. 1), began in the 1960s and focused on ancient Maya impact on regional watersheds as well as Holocene climate change and its implications for Maya civilization (Cowgill *et al.,* 1966; Deevey *et al.,* 1979; Rice *et al.,* 1985; Vaughan *et al.,* 1985; Binford *et al.,* 1987; Leyden, 1987; Brenner *et al.,* 1990; Islebe *et al.,* 1996; Beach *et al.,* 2006; Anselmetti *et al.,* 2007). By the late 1970s, Deevey and colleagues had begun searching for Pleistocene-age deposits in the Maya heartland to gain insights into Ice-age climate shifts in the lowland Neotropics (Deevey *et al.,* 1983; Leyden, 1984; Leyden *et al.,* 1993, 1994). Attention was focused on relatively deep lakes, as most shallow basins in the region were shown to have first filled with water in the early Holocene and were evidently dry during glacial times. Recent palaeoenvironmental studies in the region have focused on obtaining even longer sediment records to investigate tropical climate and environmental changes on the Yucatan Peninsula during both glacial and interglacial times, and to explore terrestrial-marine linkages using palaeoclimate records from sites around the Caribbean (for example, Cariaco Basin, north of Venezuela; Haug *et al.,* 2001). Retrieval of long sediment cores from the Neotropical lowlands became a major objective for palaeoenvironmental and palaeoclimatological studies. Until the present study, the longest lacustrine sediment record taken in the region was a core from relatively deep (z_{max} = 32 m), small (area = 2·2 km^2) Lake Quexil. Collected in 1980, the core penetrated *ca* 20 m below the sediment–water interface. Unfortunately, the Pleistocene-age section of the sequence was poorly dated. Pleistocene deposits contained few terrestrial macrofossils, and the estimated basal age of the core (36 ka) was based on extrapolation of a radiocarbon date from an aquatic snail shell (Leyden *et al.,* 1993). For more than two decades, the Quexil core was
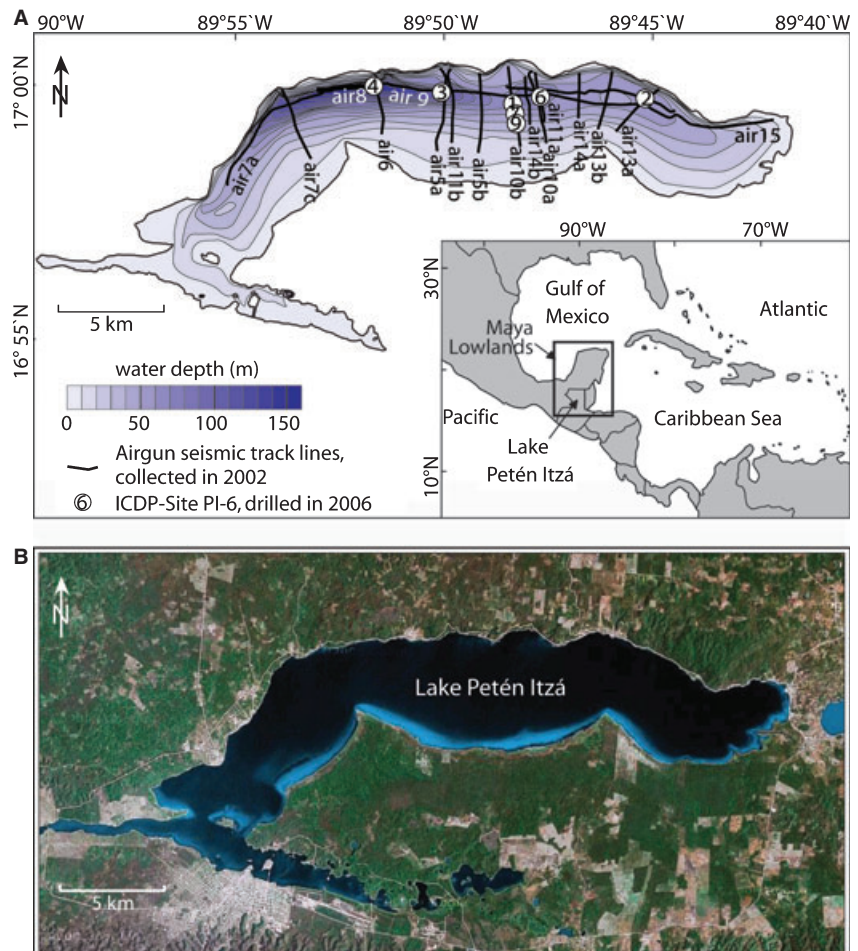

Fig. 1. (A) Bathymetric map of Lake Petén Itzá showing the locations of all ICDP sites drilled in 2006, and of all seismic track lines collected in the 2002 airgun seismic reflection survey. The inset on the right displays a map of the Caribbean region showing the Maya Lowlands in northern Guatemala and the location of Lake Petén Itzá. (B) Satellite picture of Lake Petén Itzá. Note the shallow water area along the south shore characterized by turquoise colour indicating *in situ* carbonate production (Mueller *et al.,* 2009).

the longest continental palaeoclimate record from the area.

Seismic reflection surveys of Lake Petén Itzá completed in 1999 and 2002 revealed the potential for obtaining a very old palaeoclimate archive from the lowlands of Guatemala (Anselmetti *et al.*, 2006). Lake Petén Itzá is the largest (*ca* 100 km^2) and deepest lake ($z_{max} > 160$ m) in lowland Central America (Hillesheim *et al.*, 2005); because of its great depth, it held water even during the driest periods of the late Pleistocene. Seismic reflection data indicated over 100 m of sediment in some depocentres (Anselmetti *et al.*, 2006). The Petén Itzá sediment record contains a unique environmental and climate archive that extends back far beyond the record from nearby Lake Quexil. Because of its excellent palaeoenvironmental potential, the sediment record of Lake Petén Itzá was drilled in spring 2006 as part of an International Continental Scientific Drilling Program (ICDP) project, using the Global Lakes Drilling (GLAD 800) platform.

More than 1300 m of lake sediment was recovered from seven locations in Lake Petén Itzá (Hodell *et al.*, 2006), hereafter referred to as sites PI-1, PI-2, PI-3, PI-4, PI-6, PI-7 and PI-9 (Fig. 1, Table 1). Results presented in this study document the full sediment record of all drill sites, which extends back >200 kyr. Sediments covering the period from 200 to 85 ka were recovered at only two sites, PI-1 and PI-7. This older succession has less age control and is probably less continuous than the younger section, which was drilled at all sites, allowing detailed palaeoenvironmental interpretations spanning the last 85 kyr (Hodell *et al.*, 2008). Interbedded clay and gypsum deposits at site PI-6 were interpreted as representing alternating humid and dry climate, deposited during high and low lake level stands, respectively (Hodell *et al.*, 2008). Details of the

climate reconstruction are presented in Hodell *et al.* (2008), but are summarized briefly here. The palaeoclimate history was inferred mainly for the last 40 kyr, the period for which the chronology is well-constrained by radiocarbon dates on terrestrial macrofossils. Clay and gypsum alternation from 40 to 23 ka [late Marine Isotope Stage (MIS) 3] appears to correlate with stadial–interstadial (IS) stages (Dansgaard-Oeschger events; Dansgaard *et al.*, 1993) from Greenland ice cores and North Atlantic marine sediment cores, as well as with precipitation proxies from the Cariaco Basin (Peterson *et al.*, 2000; Haug *et al.*, 2001). Gypsum units are associated with cold stadials, especially those containing Heinrich Events, whereas clay units are related to warm IS. An unexpected finding was that sediments deposited in Petén Itzá during the Last Glacial Maximum (LGM), from *ca* 23 to 18 ka, consist of a thick clay unit; this suggests substantial detrital input and a high lake level, hence, more humid climate conditions during the LGM, compared to the preceding and succeeding periods in Petén (Hodell *et al.*, 2008; Bush *et al.*, 2009). This finding contradicts previous palaeoclimate interpretations that proposed a dry LGM in the lowland Neotropics of Central America. The driest period of the last glaciation was not the LGM, but rather the deglacial period (*ca* 18 to 11 ka), when lake level fluctuated between low and intermediate stands, as indicated by alternating gypsum and clay sediments.

Following the preliminary palaeoclimate interpretations of Hodell *et al.* (2008), a basin-wide stratigraphy of the Lake Petén Itzá sediment record is constructed by integrating data from all drill sites. Furthermore, previously collected seismic reflection data of Anselmetti *et al.* (2006) are combined with new lithological data from the drill cores to test and improve the proposed

Table 1. Location of drill sites, penetration depth (metres below lake floor), and percent recovery for cores collected in Lake Petén Itzá.

Site	Latitude	Longitude	Water depth (m)	Penetration depth (mblf)					Average recovery
				Hole A	Hole B	Hole C	Hole D	Hole E	
PI-1	16°59·97′ N	89°47·74′ W	65	94·5	90·3	82·5			89·3
PI-2	16°59·97′ N	89°44·69′ W	54	66·5	41·2	82·4	42	68·5	86·3
PI-3	17°0·20′ N	89°49·24′ W	100	96·9	95·3	90			92·9
PI-4	17°0·33′ N	89°50·77′ W	150	67·4	46·1	25·4			86·7
PI-6	17°0·02′ N	89°47·09′ W	71	75·9	66·4	66·8			94·9
PI-7	16°59·72′ N	89°47·68′ W	46	133·2	122·8	63·8			92·1
PI-9	16°59·44′ N	89°47·65′ W	30	16·4					91·8

depositional model for Lake Petén Itzá. The combination of seismic, sedimentological, geophysical and chronological data (49 AMS-^{14}C ages and a suite of identified tephra layers) facilitates understanding of the sedimentation processes that generated the lithological succession in Lake Petén Itzá, and provides information about how the lake sediments were affected by climate and environmental changes.

STUDY SITE

The Petén Lake District lies in the Neotropical lowlands of Petén, northern Guatemala, and consists of a series of lake basins oriented east–west along *en echelon* faults (Vinson, 1962). The largest and deepest lake is Petén Itzá (*ca* 16°55′ N, 89°50′ W), with its surface area of *ca* 100 km^2 and a maximum water depth >160 m (Fig. 1). Lake Petén Itzá occupies a closed basin and its volume changes in response to shifts in the balance between evaporation and precipitation. Lake Petén Itzá has a large, deep northern basin and a small, shallow southern basin. The latter has a mean water depth of only *ca* 5 m. The north shore is characterized by steep-sloping lower Tertiary limestone. The southern shore is gently sloping and, in places, rimmed by poorly drained seasonal swamps (*bajos*). The water of Lake Petén Itzá is dilute (11·2 meq l^{-1}, 408 mg l^{-1}) and is dominated by calcium and bicarbonate, with magnesium and sulphate following closely in concentration (Hillesheim *et al.*, 2005). Lake water pH is high (*ca* 8·0) and is saturated with respect to calcium carbonate. The oxygen isotopic composition (δ^{18}O) of lake water averages +2·9‰, which is enriched by *ca* 7‰ relative to regional rainfall and groundwater (*ca* −4‰) (Hillesheim *et al.*, 2005); this reflects the importance of evaporation in the water budget of the lake. Thermal stratification persists through most of the year, with hypolimnetic temperatures *ca* 25·4 °C, close to the mean annual air temperature. Surface sediments in the littoral zone of Lake Petén Itzá are rich in gastropods (mainly *Tryonia* sp. and *Cochliopina* sp.) and poor in ostracods, whereas sediments in deep water contain few gastropods, but are rich in ostracods (mainly *Candona* sp. and *Cytheridella ilosvayi*). Surficial sediments down to a water depth of *ca* 23 m consist of shell-rich carbonate (Mueller *et al.*, 2009). Carbonate content decreases in greater water depths where surface sediments contain higher amounts of organic matter and non-carbonate detrital constituents.

METHODS

Two seismic reflection campaigns of the Lake Petén Itzá sediment were undertaken. In 1999, a shallow, high-resolution survey (3·5 kHz pinger) was carried out and in 2002, a deeper, lower-resolution survey (1 in^3 airgun) was completed (Anselmetti *et al.*, 2006). Applying a seismic sequence stratigraphic approach (Vail *et al.*, 1977) to these data, two shallow-water sites (PI-9 and PI-7), three intermediate-water-depth sites (PI-1, PI-2 and PI-6) and two deep-water sites (PI-3 and PI-4) were chosen for drilling (Fig. 1, Table 1). Seven sites were drilled in early 2006. Multiple holes were drilled at most sites (Table 1), and cores were logged in the field for density, p-wave velocity and magnetic susceptibility using a GEOTEK multi-sensor core logger (Geotek Limited, Daventry, Northants, UK). To verify complete stratigraphic recovery, the software program 'Splicer', which allows alignment of lithological features among holes using core-logging data (i.e. density and magnetic susceptibility), was used. Depths in the cores are reported in metres below lake floor (mblf), or where established, in metres composite depth (mcd), which represents a complete composite section using cores from multiple holes at the same site.

The chronology for the last 40 kyr of the Lake Petén Itzá sediment record was developed using 21 AMS-^{14}C dates from site PI-6, 10 AMS-^{14}C dates from site PI-3 and 18 AMS-^{14}C dates from site PI-2, all measured on samples of terrestrial organic matter (Table 2). The terrestrial material was primarily wood fragments, which are unaffected by hard water dating error (Deevey *et al.*, 1954; Stuiver & Polach, 1977). Dates were converted to calendar years before 1950 (cal yr BP) using the online radiocarbon calibration program of Fairbanks *et al.* (2005) (http://radiocarbon.ldeo.columbia.edu/research/radcarbcal.htm).

Ages are reported in calibrated thousands of years (ka) before 1950. Sediments older than 40 ka were dated by identification of tephra layers within the Petén Itzá cores that were geochemically fingerprinted (microprobe analysis) and matched with the established onland tephrochronology for Central America after Kutterolf *et al.* (2007, 2008a) (Table 3). The presence of lithological markers, stratigraphic boundaries and tephra layers, as well as the very similar magnetic susceptibility and bulk density records throughout the basin, allowed layer-to-layer correlation between most sites. This correlation enabled

Table 2. Radiocarbon dates on terrestrial organic material (woody debris) from sites PI-2, PI-3 and PI-6. All radiocarbon dates were converted to calendar years with the on-line radiocarbon calibration program (Fairbanks *et al.*, 2005): http://radiocarbon.ldeo.columbia.edu/research/radcarbcal.htm. Reporting of ages follows the convention of Stuiver & Polach (1977).

Accession no. CAMS	Sample Site hole–Core type– section, interval	Depth (mcd)	Age ^{14}C yr BP	± (1σ)	Age cal yr BP	± (1σ)
139341	2D–2H–2, 25 cm	4·88	1715	35	1620	50
139342	2B–4H–2, 39 cm	10·54	3705	30	4040	50
139416	2B–4H–2, 39 cm rep	10·54	3775	35	4140	50
139344	2B–5H–1, 102 cm	11·14	7455	35	8290	50
139417	2B–5H–1, 102 cm rep	11·14	7480	45	8320	50
139346	2D–5H–1, 56 cm	13·05	7835	30	8600	30
139345	2B–6H–2, 41 cm	16·71	11 135	40	12 990	40
139399	2D–6H–2, 44 cm	17·74	11 880	35	13 720	50
139400	2D–8H–1, 5 cm	21·91	13 480	45	15 690	120
139401	2B–8H–1, 132 cm	22·13	13 505	45	15 720	120
139418	2B–8H–1, 132 cm rep	22·13	13 560	45	15 780	120
139402	2B–9H–1, 146 cm	25·74	15 355	50	18 600	70
139403	2B–12H–1, 121 cm	34·43	25 540	160	30 700	200
139404	2A–14H–1, 115 cm	38·66	32 680	980	38 100	1000
139405	2A–16H–1, 66 cm	44·83	34 380	450	39 700	500
139406	2C–2H–1, 135 cm	47·32	38 760	740	43 600	700
139407	2A–17H–1, 104 cm	48·17	41 350	1020	45 900	900
139343	2A–17H–1, 151 cm	48·35	41 600	900	46 100	800
128603	3B–2H–1, 93 cm	4·23	2140	40	2130	70
128604	3A–3H–2, 17 cm	9·37	4590	40	5310	70
128614	3A–3H–2, 17 cm rep	9·37	4550	35	5250	80
128605	3C–4H–2, 140 cm	11·32	8625	35	9560	20
128615	3C–4H–2, 140 cm rep	11·32	8675	35	9600	50
128606	3B–5H–2, 25 cm	14·17	11 210	35	13 020	40
128607	3A–9H–1, 71 cm	28·09	23 210	90	27 850	170
128616	3A–9H–1, 71 cm rep	28·09	23 040	90	27 650	170
128608	3B–10H–1, 144·5 cm	30·09	26 560	130	31 800	200
128609	3B–11H–2, 9·5 cm	33·42	32 820	260	38 200	300
125895	6C–3H–1, 141·5 cm	8·08	3920	35	4380	50
125903	6C–3H–1, 141·5 cm	8·08	3905	35	4360	60
125896	6B–4H–2, 77·5 cm	10·41	8655	30	9580	30
125904	6B–4H–2, 77·5 cm	10·41	8630	60	9570	50
131225	6C–4H–1, 59 cm	10·44	7985	40	8880	100
131226	6C–4H–1, 101 cm	10·86	9040	35	10 210	20
128611	6B–5H–2, 33 cm	13·35	11 290	60	13 130	70
128613	6B–5H–2, 39 cm	13·41	11 380	140	13 230	150
131224	6B–5H–2, 85 cm	13·87	11 390	50	13 240	70
128612	6C–5H–2, 7 cm	14·45	12 460	60	14 400	150
131223	6C–6H–1, 120 cm	17·12	12 280	60	14 080	100
125897	6A–7H–1, 128 cm	20·03	14 130	120	16 540	210
125898	6C–8H–2, 6 cm	23·64	17 650	240	20 900	320
125899	6C–9H–1, 62 cm	25·73	19 990	180	23 880	220
125900	6A–11H–2, 145 cm	33·73	30 700	3600	36 000	3700
125901	6B–12H–1, 82·5 cm	33·83	29 120	170	34 500	200
125905	6B–12H–1, 82·5 cm	33·83	29 010	170	34 400	200
126525	6B–12H–1, 138·5 cm	34·39	28 040	470	33 400	500
126526	6C–14H–1, 80·5 cm	41·3	39 000	700	43 900	600
126527	6A–15H–2, 90·5 cm	45·31	38 100	1100	43 100	1000
126528	6B–15H–1, 60 cm	42·76	35 900	1200	41 100	1100

extrapolation of dates from site to site, yielding a detailed age-depth model for the entire sediment record of Lake Petén Itzá (Figs 2 and 3).

Lithological units were defined by sediment types, which were established following the classification scheme of Schnurrenberger *et al.*

Table 3. Lake Petén Itzá sediment tephrochronology.

Tephra	Sample Site hole–core type–section, position (cm)	Depth (mcd)	Age (cal yr BP)	Dating method
Congo Tephra (CGT)	6C–17E–2, 22 1B–15H–2, 78 7A–15H–1, 73	51·3 37·0 25·0	53 ± 3 ka	Dated by ^{14}C (Kutterolf *et al.*, 2008a)
Guatemala–El Salvador Tephra 1 (Guasal1)	6A–18E–3, 126 2C–9H–1, 114 1B–16H–1, 58	52·7 64·8 38·0	*ca* 55 ka	Dated by stratigraphic interpolation
Arce Tephra (ACT)	6B–19E–2, 113 1B–16H–2, 76	55·3 39·6	72 ± 3 ka	Dated by Ar/Ar (Rose *et al.*, 1999)
Los Chocoyos Tephra (LCY)	6A–24E–2, 49 1B–20H–3, 58	70·9 51·0	84 ± 0·5 ka	Dated by oxygen isotope stratigraphy (Rose *et al.*, 1999)
W-Tephra (WFT)	7A–30E–3, 84	74·3	158 ± 3 ka	Dated by Ar/Ar (Rose *et al.*, 1999)
L-Tephra (LFT)	1A–27H–2, 128	84·3	191 ± 11 ka	Dated by Ar/Ar (Rose *et al.*, 1999)

(2003). Sediment samples were taken at selected depths for analysis. Smear slides were prepared and studied with scanning electron microscopy. Grain-size distribution was established using laser diffraction techniques. Mineralogical composition was determined by applying the Rietveld technique to measured X-ray diffraction (XRD) patterns (Ufer *et al.*, 2008). The Rietveld technique is a full pattern-fitting method that consists of the calculation of the X-ray diffractogram and its iterative adjustment to the measured XRD-pattern by refinement of phase specific parameters (Young, 2002).

RESULTS

Core recovery and sediment chronology

A total of 1327 m of lake sediment was recovered from seven sites, with an average core recovery of 90·6% (Table 1). Samples of terrestrial organic matter in Petén Itzá sediments, dated by radiocarbon, yielded reliable chronologies for deposits younger than 40 ka. Most ages are in depth order (Hodell *et al.*, 2008; Table 1; Fig. 2). Selected tephra layers in Petén Itzá sediments >40 ka were compared to the existing Central American tephra stratigraphy (Kutterolf *et al.*, 2008a; Table 3). In PI-6, the CGT Tephra (*ca* 53 ka) is at 51·3 mcd, the Guasal1 Tephra (*ca* 55 ka) is at 52·7 mcd and the ACT Tephra (*ca* 72 ka) is at 55·3 mcd (Table 3). The depth of the ACT tephra suggests a consider-

able change in sedimentation rate, and was not included in the age-depth model. The age of the base of the PI-6 core is constrained by an ash layer at 70·9 mcd from the *ca* 84 ka Los Chocoyos (LCY Tephra) eruption of the Atitlán Caldera in the Guatemalan highlands (Rose *et al.*, 1999; Kutterolf *et al.*, 2007). This LCY ash layer occurs at 51·0 mcd in site PI-1 (Fig. 2), implying that sediments below this marker horizon in PI-1 are much older than 84 ka. Thus, the PI-1 core contains a much longer record than does PI-6. Indeed, the WFT ash layer, dated at *ca* 158 ka, was identified at 72·0 mcd in PI-1 (Table 3; Fig. 2; Rose *et al.*, 1999; Kutterolf *et al.*, 2008a). The same ash layer was also identified in shallow-water core PI-7 at 74·3 mcd (Fig. 3). Cores from PI-1 and PI-7 have much older records than do any of the other sites. At 84·2 mcd in site PI-1, ash from the *ca* 191 ka LFT eruption of Amatitlan was identified (Table 3; Fig. 2; Rose *et al.*, 1999; Kutterolf *et al.*, 2008a), suggesting a basal age of *ca* 200 ka. Shallow-water site PI-7, which penetrated to 133·2 m, contains no identifiable ash layer in the 60 m below the WFT tephra. The sedimentation rate, down to an age of *ca* 53 ka (CGT tephra), averages *ca* 1·0 mm year^{-1} in site PI-6, *ca* 0·7 mm year^{-1} in site PI-1 and *ca* 1·2 mm year^{-1} in site PI-2 (Fig. 2). Below the CGT tephra in cores from PI-6 and PI-1, sedimentation rates were somewhat lower, *ca* 0·6 mm year^{-1} and *ca* 0·4 mm year^{-1}, respectively (Fig. 2). In site PI-2, the sedimentation rate remained relatively constant throughout, *ca* 1·2 mm year^{-1}.
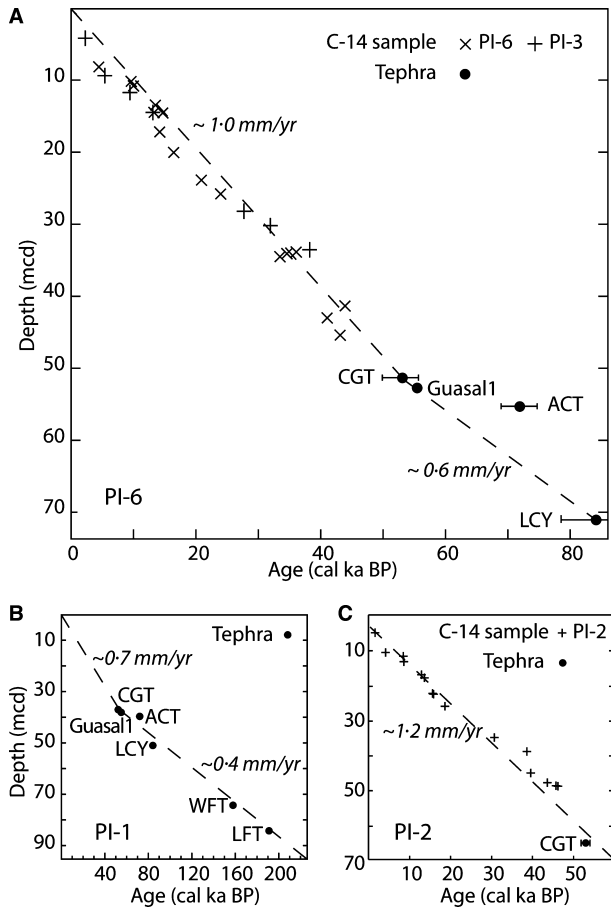
Fig. 2. Calibrated ages (cal yr BP) versus depth (mcd) of sites PI-6 (A), PI-1 (B) and PI-2 (C) showing linear approximation for sedimentation rates (dashed lines). Ages younger than 40 ka are derived by radiocarbon dating of samples from terrestrial organic matter. Ages older than 40 ka are dated by characteristic tephra layers from volcanic eruptions of known age (Table 3). The dating error on all samples is smaller than the plot symbols, except where indicated by an error bar.

Sediment types

Seven main sediment types ([A] clastic lacustrine, [B] precipitated, [C] microbial, [D] pyroclastic, [E] clastic terrestrial, [F] karstic/soil, [G] bedrock) were identified, together with several additional sub-types in the case of [A] and [B] (Table 4; Fig. 4). Each sediment type, and its sub-types, is described (Table 4) and photographed (Fig. 4). Table 4 contains the palaeoenvironmental interpretations for the sediment types.

Lithostratigraphic units

The different sediment types (Table 4) were used to divide the sediment record of Lake Petén Itzá into 11 lithostratigraphic units, labelled I to IX,

Basal Gravel Unit (BGU), Mottled Unit (MU) and into sub-units labelled with lower-case letters, for example, IVa (Fig. 3), which overlie the basement of Lake Petén Itzá. Using core-logging data (density and magnetic susceptibility) and characteristic lithological layers in split cores along seismic reflection profiles, most of the lithostratigraphic units can be correlated from site to site throughout the entire basin (Figs 3 and 5 to 7). In general, the recovered sediment cores provide an undisturbed succession of the depositional history. In some cases, however, especially at deep-water sites, there are structures in the sediment fabric that indicate down-slope movement and re-deposition of sediments into basinal areas (Fig. 8). Such movements often occur along tephra layers with low shear strength and gliding surfaces (Fig. 8). This phenomenon was described previously from the Central American Forearc, where large submarine slides of the last 100 kyr were often associated with tephra layers (Harders *et al.*, 2007; Kutterolf *et al.*, 2008b). These mass movements did not prevent establishment of a stratigraphic framework as they were easily identified in seismic and core data. Here, results are presented in order from youngest to oldest deposits, i.e. from top to bottom.

Unit I (0 to 10 ka)

Unit I is a thick sediment succession deposited during the last 10 kyr. It consists primarily of grey, sub-millimetre, laminated montmorillonite-carbonate mud [A1], with reworked fragments of gastropods. Minerals such as dolomite, pyrite, quartz and feldspars are scarce or poorly developed and give weak and ambiguous XRD signatures. Unit I sediments include dark and graded calcite-montmorillonite silt-turbidites [A3] (Fig. 9) and thin, white, graded carbonates and turbidites [A2]. Magnetic susceptibility values are moderately high, reaching values between 20 and 30×10^{-6} SI. Much of this thick detrital clay unit was previously named 'Maya Clay', and is labelled here as sub-unit 'I$_m$' (site PI-6 in Figs 3 and 10). This 'Maya Clay' has been identified in many Petén lakes, and is attributed to accelerated soil erosion resulting from ancient Maya land clearance between *ca* 1·0 and *ca* 3·0 ka (Deevey *et al.*, 1979; Binford *et al.*, 1987; Brenner, 1994; Rosenmeier *et al.*, 2002; Anselmetti *et al.*, 2007).

Unit II (10 to 18 ka)

Sediments of Unit II were deposited during the last deglaciation between 10 and 18 ka. Unit II is sub-divided into three gypsum-rich sub-units [B]
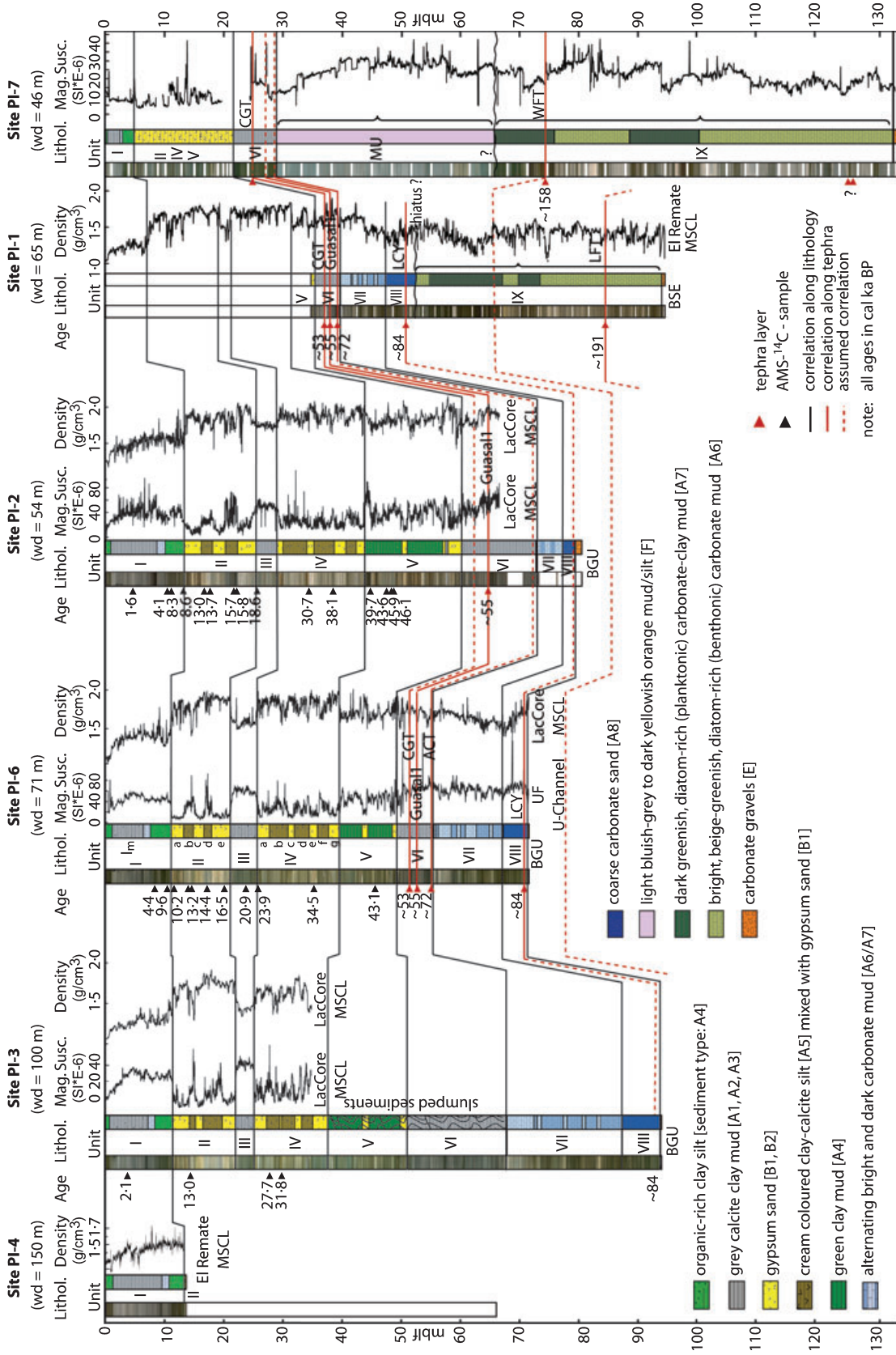
Fig. 3. Compiled data set of drill sites of Lake Petén Itzá (for site locations, see Fig. 1). Each site is documented (from left to right) by ages (in cal ka BP; for errors, see Table 2), photographic images, the stratigraphic column, lithological units (roman numerals indicate lithostratigraphic units; MU, Mottled Unit; BGU, Basal Gravel Unit; BSE, basement), the records of magnetic susceptibility (SI × 10^{-6}) and/or of the bulk density (g cm^{-3}). Core-to-core correlations along unit boundaries are indicated by black lines, correlations of characteristic tephra layers are delineated by red lines and dashed lines are assumed correlations. The depth scale for all sites is metres composite depth (mcd) except for site PI-7 where it is metres below lake floor (mblf) as indicated.

Table 4. Lake Petén Itzá sediment types.

Sediment type	Dominant mineralogy/ composition	Sedimentary structures	Interpretation/depositional environment
A. Clastic lacustrine sediment types			
A1. Grey mud	Montmorillonite, calcite	Very homogenous, extremely fine-grained clay, sub-millimetre laminations; rich in fragments of reworked gastropods	Detrital input of eroded soil and weathered limestone in the watershed
A2. White sand	Calcite	Millimetre to centimetre-thick fining upward silty sand sequences	Turbidites derived from slope instabilities in the shallow-water carbonate zone
A3. Dark, grey silt-sand	Montmorillonite, calcite	Graded fining-upward sequences (up to 5 cm thick) characterized by: (i) colour gradients from a dark grey base to a light grey top; (ii) upward-decreasing density; and (iii) sharp, irregular contacts at the base	Turbidity currents transporting eroded soil from the watershed during flood events
A4. Dark green clay mud-silt	Montmorillonite, organic matter	Homogenous clay mud with sub-millimetre laminations. Rich in planktonic diatoms (*Aulacoseira* sp.)	Deep-water, pelagic environment, low water energy
A5. Cream-coloured silt	Montmorillonite, calcite	Massive to weakly laminated silt	Detrital input from eroded soil and limestone in the watershed
A6. Bright, beige mud	Calcite	Finely laminated (millimetre-scale) mud with some euhedral calcite crystals; rich in benthonic diatoms (*Mastogloia, Denticula*)	Shallow-water to sub-littoral environment, rarely authigenic precipitation
A7. Dark, brown-greenish mud	Calcite, montmorillonite	Homogenous, finely laminated, organic-rich mud; rich in planktonic diatoms (*Aulacoseira* sp.)	Deep-water to sub-littoral environment
A8. Beige-greenish silt-sand	Calcite	Poorly sorted carbonate sand, interbedded by up to 5 mm thick fining-upward graded sand sequences; wood remains; rich in fragments of carbonate shells	$CaCO_3$ production in high-energy environment of the littoral zone

Table 4. Continued

| Sediment type	Dominant mineralogy/composition	Sedimentary structures	Interpretation/depositional environment
B. Precipitated sediment types			
B1. Brownish to yellowish sand of gypsum crystals	Gypsum	Centimetre to decimetre-thick, massive to weakly laminated (centimetre-scale) sequences composed of euhedral, large (up to 5 mm) gypsum crystals	Authigenic precipitation
B2. Yellowish gypsum nodules	Gypsum	Undulating laminations of gypsum lenses (up to 1 cm long) with concretions of gypsum nodules	Authigenic deposits in littoral zones during high-salinity periods (Valero Garcés & Kelts, 1995)
C. Microbial sediment type			
C. White, yellowish sulphur nodules	Sulphur	Cross-cutting bedding of clay and gypsum sediments. Typically occurring at transitions from gypsum to clay units	Nodules were formed post-depositionally as they crosscut bedding
D. Pyroclastic sediment type			
D. Black or white ash layers	Transparent to brownish glass shards	Dry and porous	Pyroclastic deposits from ashfall, partly reworked
E. Clastic terrestrial sediment type			
E. Gravel-rich sand	Limestone gravels, terrestrial gastropods	Limestone gravels in a coarse, carbonate sand matrix	Sediments deposited during a very low lake level stand. Deposited in a beach-like environment
F. Karstic/soil sediment type			
F. Mottled, light bluish grey to dark yellowish orange mud-silt	Montmorillonite, calcite, pyrite	Structureless and sticky, light bluish grey to dark yellowish orange, fine-grained sediments	Formed under wet, anaerobic conditions (moor-like) and under the presence of anaerobic micro-organisms. Gley-like formation?
G. Bedrock			
G. White, beige, angular limestone pieces (recovered only in sites PI-1 and PI-7)	Carbonates	Structureless, fine-grained limestone pieces within a coarse sand carbonate matrix	Limestone of the Cretaceous to Tertiary carbonates from the bedrock
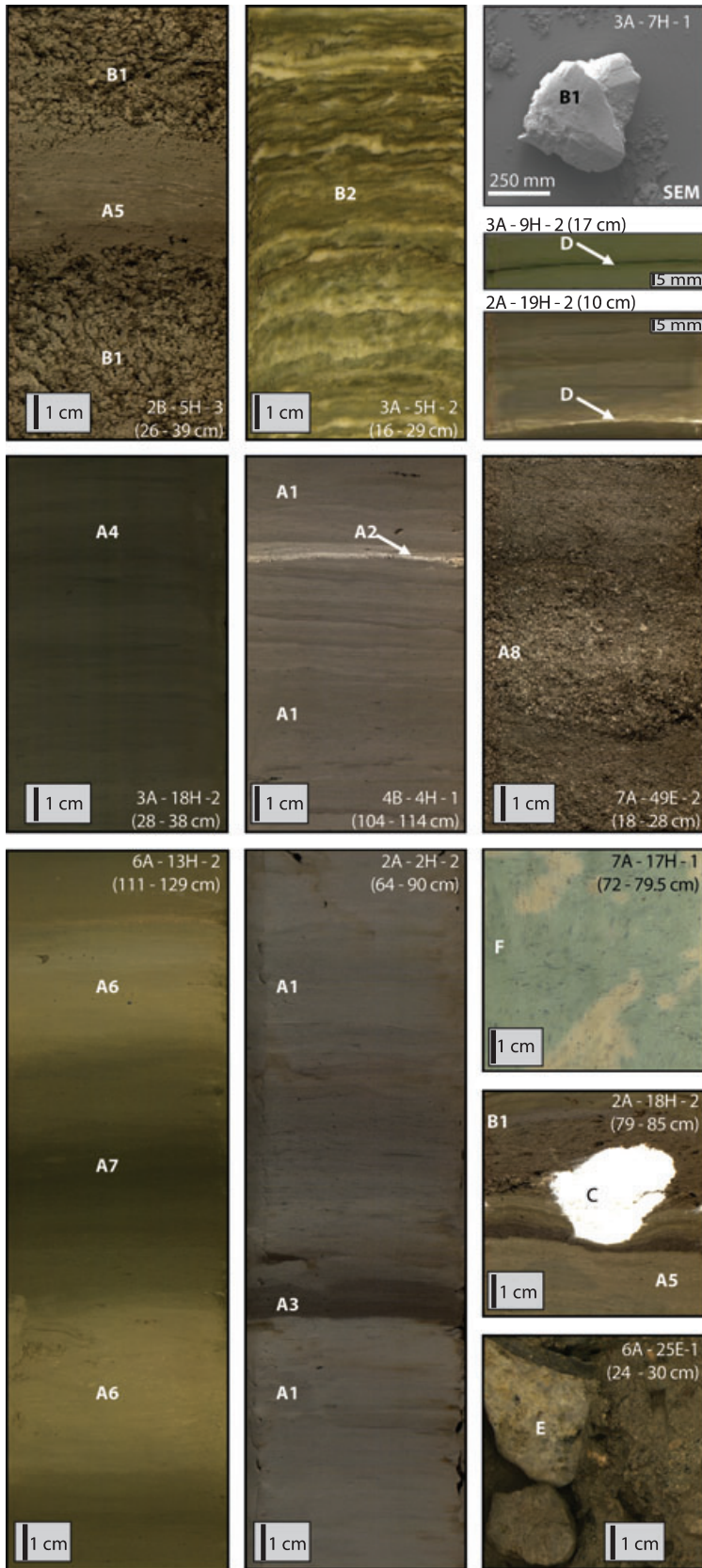
Fig. 4. Core photographs showing different sediment types (indicated by capital letters) including a scanning electron micrograph of an idiomorphic gypsum crystal (upper right panel). For explanations of the sediment types, see Table 4.
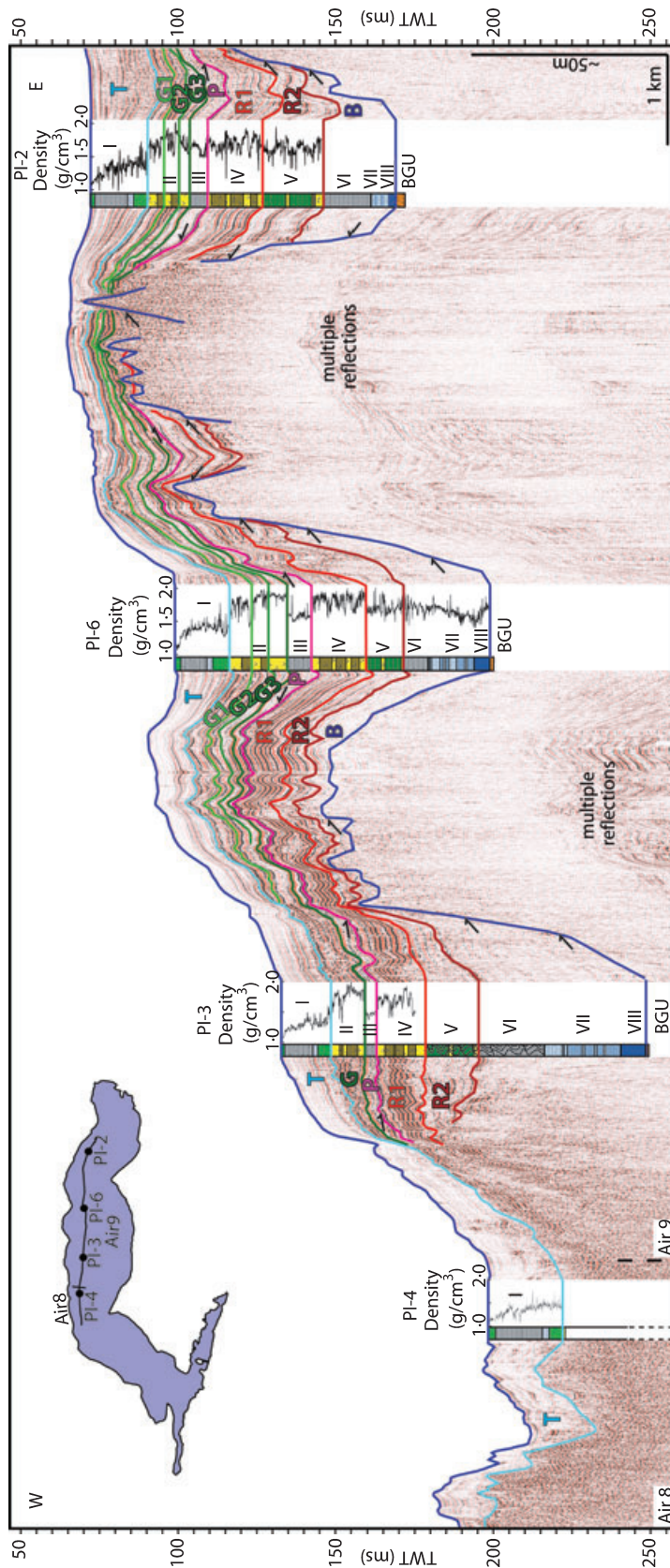
Fig. 5. Seismic-to-core correlation of sites PI-4, PI-3, PI-6 and PI-2 along an E–W basin-parallel reflection seismic profile composed of two seismic lines (Air8 and Air9). The seismic sequences are labelled with coloured capital letters: T(urquoise), G(reen), P(ink), R(ed) and B(lue). Sub-sequences are indicated by numerals 1 to 5. The small lake inset map displays the location of seismic tracks Air8 and Air9, and the location of imaged sites. For colour-coding of the lithological column, see Fig. 3.
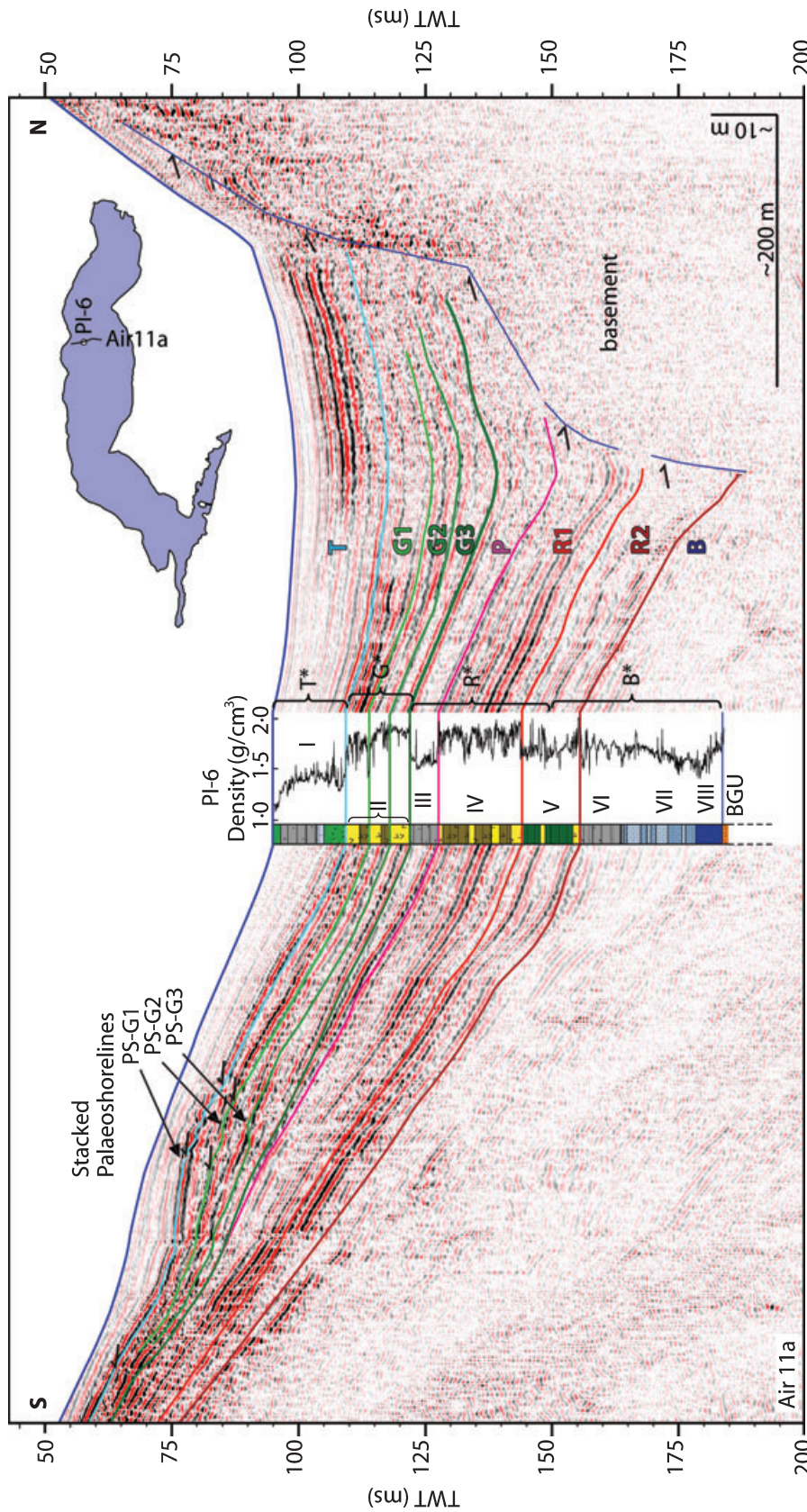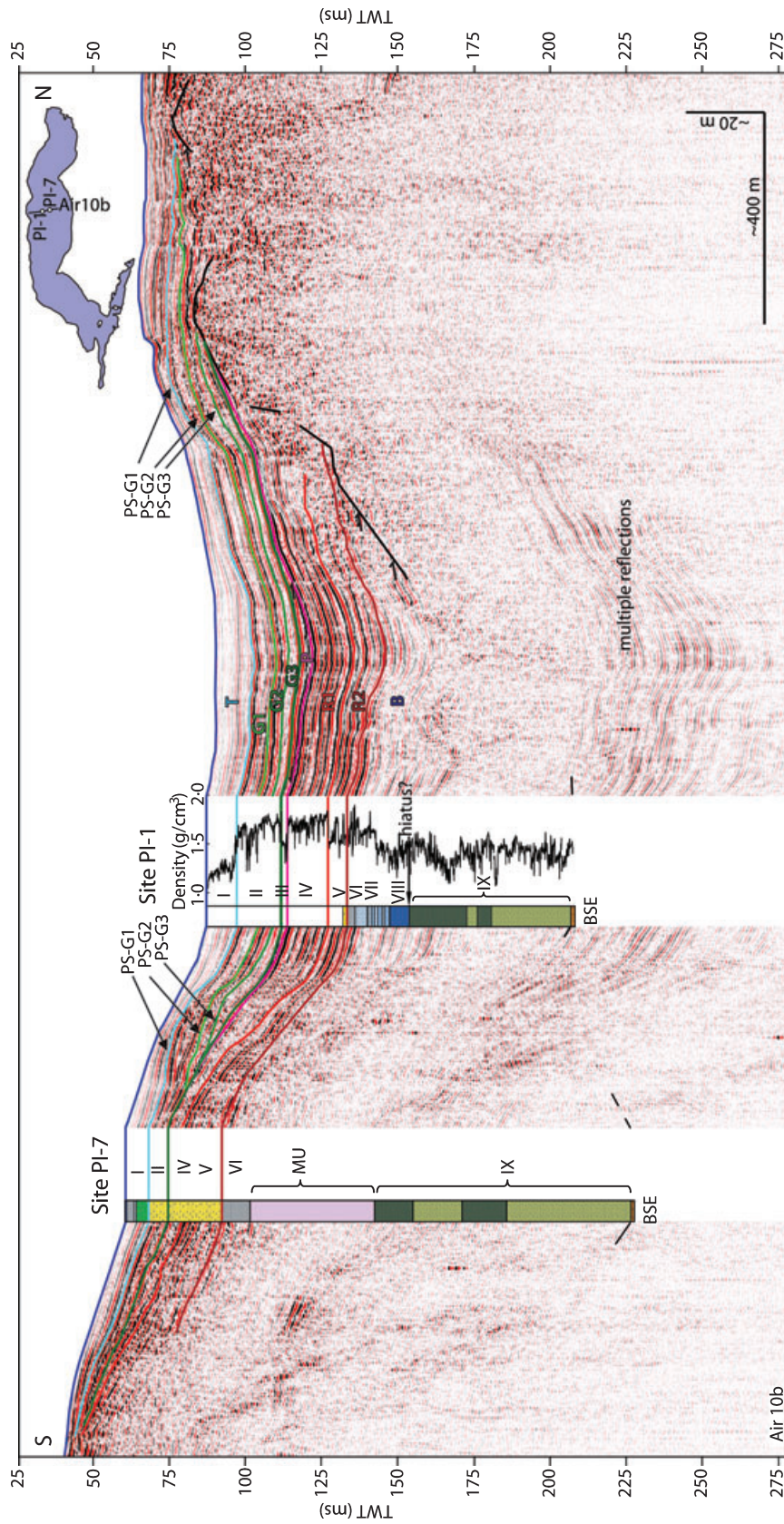
Fig. 6. Seismic-to-core correlation of site PI-6 along the cross north–south reflection seismic profile Air11a. The seismic sequences are labelled with coloured capital letters T(turquoise), G(reen), P(ink), R(ed) and B(lue). Sub-sequences are indicated by numerals 1 to 5. In black capital letters with *: earlier interpretation of Anselmetti *et al.* (2006). Small lake inset map displays the location of seismic track Air 11a, and the location of site PI-6. Note the occurrence of three stacked palaeoshorelines, each of which corresponds to the top of a gypsum layer in lithological Unit II of site PI-6 deposited during the Late Glacial. For symbol legend, see Fig. 3.

Fig. 7. Seismic-to-core correlation of sites PI-1 and PI-7 along the cross N–S reflection seismic profile Air10b. Seismic sequences are labelled with coloured capital letters: T(urquoise), G(reen), P(ink), R(ed) and B(lue). Sub-sequences are indicated by numerals 1 to 5. The small lake inset map displays the location of seismic track Air 10b, and the location of sites PI-1 and PI-7. For symbol legend, see Fig. 3.
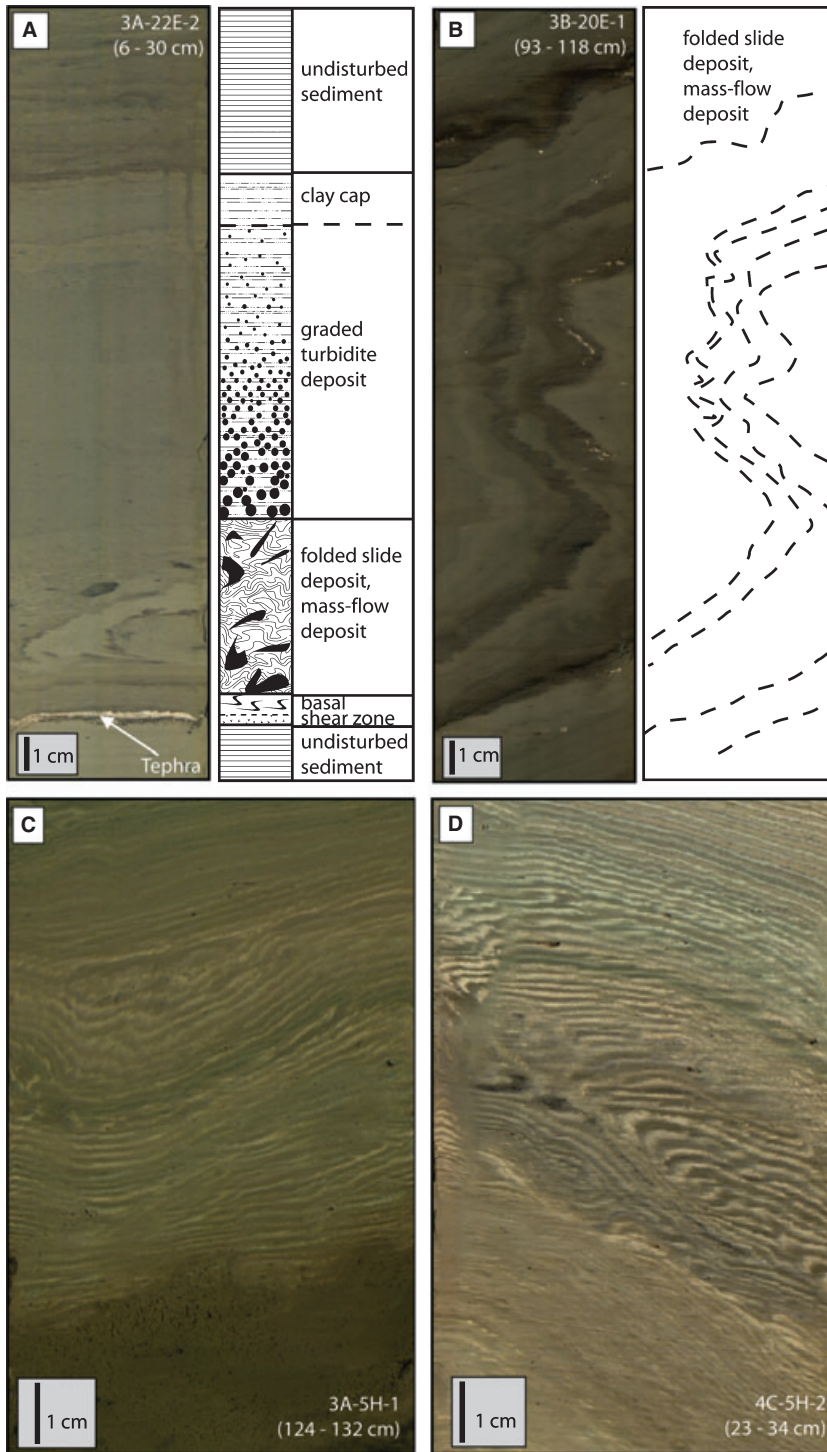
Fig. 8. Core photographs showing disturbed mass-flow deposits and folded laminated sediments in Lake Petén Itzá. (A) Turbidite deposit in Unit VI (sediment type A1): basal tephra layer acting as a shear plane horizon, overlain by folded slide deposits, a graded fining-upward sequence and a fine homogenous clayey cap. (B) Slumped mass-flow deposit in Unit VI (sediment type A1). (C) Folded sub-millimetre lamination in Unit I (sediment type A4). (D) Folded sub-millimetre lamination in Unit II (sediment type A5).

IIa (11·5 to 12·8 ka), IIc (13·5 to 14 ka) and IIe (15 to 18 ka), and two clay-rich carbonate sub-units (A5) IIb (12·8 to 13·5 ka) and IId (14 to 15 ka) (Fig. 3). Gypsum-rich sub-units consist of brown to yellowish massive accumulations of coarse, authigenic gypsum crystals [B1], and/or undulating finely laminated, yellowish nodular gypsum layers [B2]. Clay-rich carbonate sub-units consist of weakly laminated calcite-montmorillonite silt [A5]. Gypsum sequences generally are characterized by low magnetic susceptibility and high density, whereas clay-carbonate sequences are represented by higher magnetic susceptibility and lower density (Fig. 3).
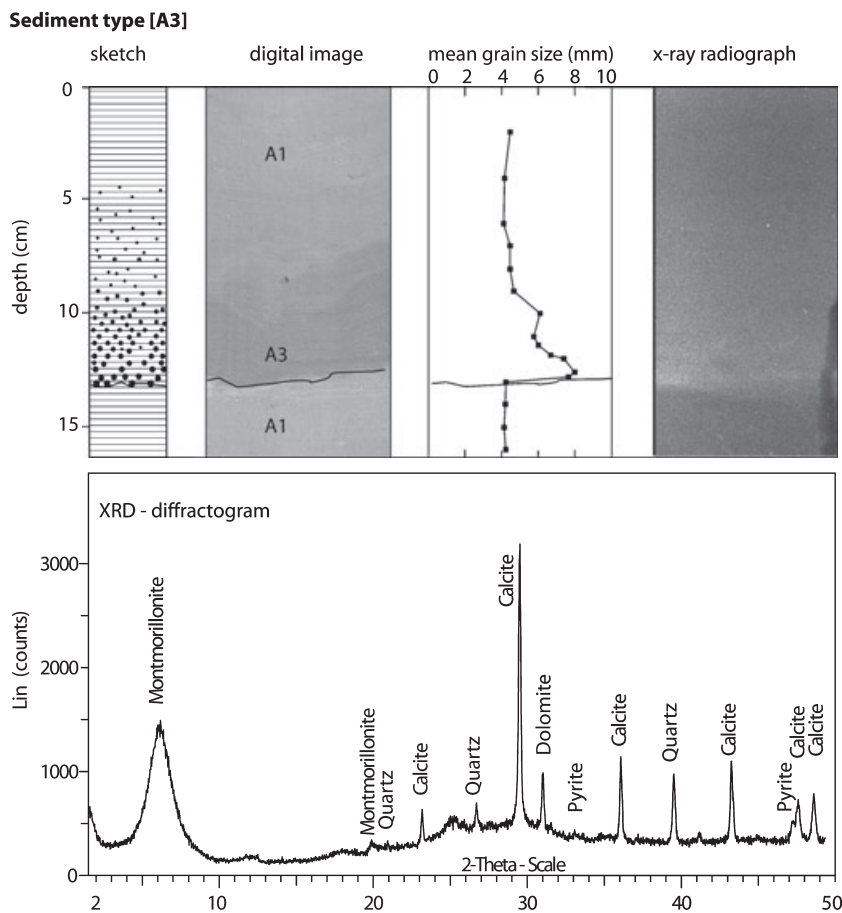
Sediment type [A3]

Fig. 9. Physical characteristics of sediment type A3. Top, from left to right: schematic sketch of a fining upward sequence, colour gradient from dark base to bright top on core photograph, fining upward of particle sizes in grain-size analysis, and upcore decreasing density record on X-ray radiograph (light colours = high density); Bottom: XRD diffractogram of sediment type A3.

Unit III (18 to 23 ka)

Unit III, deposited between 18 and 23 ka, coincides approximately with the LGM (Mix *et al.*, 2001). This unit is characterized by grey, submillimetre-scale laminated mud, consisting mainly of montmorillonite and calcite [A1]. Dolomite, pyrite, quartz and feldspar occur as trace minerals. Fragments of reworked gastropods are common in this unit. The finely laminated clay is often interbedded by dark grey, graded silt sequences with irregular and erosive bases [A3]. These graded sequences vary in thickness between 1 and 3 cm. Throughout Unit III, magnetic susceptibility is high (40 to 60×10^{-6} SI), whereas density is low (<1·5 g cm^{-3}) (Fig. 3).
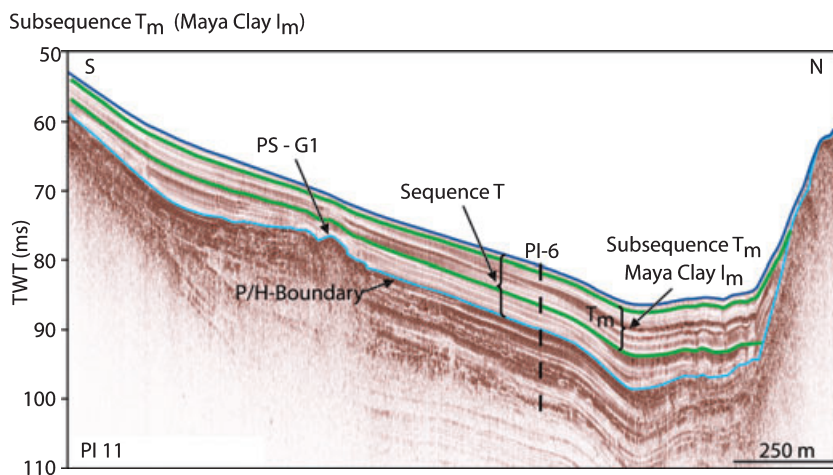

Fig. 10 High-resolution seismic N-S profile (Pinger line PI 11) documenting seismic sub-sequence T_m coinciding with lithological sub-unit I_m ('Maya Clay'). P/H boundary, Pleistocene/Holocene transition; PS-G1, palaeoshoreline G1.

Unit IV (23 to 39 ka)

The sediments of Unit IV accumulated between 23 and 39 ka. Unit IV is sub-divided into four gypsum-rich sub-units: IVa (23 to 25 ka), IVc (30 to 32 ka), IVe (35 to 36 ka) and IVg (38 to 39 ka), and three clay-rich carbonate sub-units IVb (25 to 30 ka), IVd (32 to 35 ka) and IVf (36 to 38 ka) (Fig. 3). Similar to Unit II, gypsum-rich sub-units consist of coarse, massive brownish-yellowish gypsum sand [B1], and/or undulating, laminated, yellowish nodular gypsum layers [B2]. Clay-rich carbonate units consist of massive, cream-coloured silt [A5]. Gypsum beds are characterized by low magnetic susceptibility and high density, whereas clay has higher magnetic susceptibility and lower density (Fig. 3).

Unit V (39 to 49 ka)

Sediments of Unit V (39 to 49 ka) consist of finely laminated, dark greenish clay mud, which is rich in organic matter [A4]. This unit consists of up to 5 cm thick, graded turbidites [A3]. Two sequences of authigenic gypsum crystals [B1, B2] were deposited, peaking at *ca* 42 and *ca* 48 ka (Fig. 3).

Unit VI (49 to 58 ka)

Sediments of Unit VI, deposited from 49 to 58 ka, are composed of grey, laminated montmorillonite mud [A1], which is partly mottled with dark, diffuse organic-rich spots. This unit is punctuated by graded, dark turbidite sequences of silt [A3]. Sediments of this unit include fragments of reworked gastropods.

Unit VII (58 to 78 ka)

Unit VII consists of sediments that were deposited from *ca* 58 to *ca* 78 ka. These sediments are composed of rhythmic alternations between bright-beige sequences of carbonate mud [A6] and darker-brown to greenish, organic-rich sequences of laminated clay-carbonate mud [A7] (Fig. 3). The darker clay bands contain planktonic diatoms (*Aulacoseira* sp.), whereas the brighter carbonate bands are rich in benthonic diatoms (*Mastogloia* and *Denticula*).

Unit VIII (78 to 85 ka)

Sediments of Unit VIII (78 to 85 ka) consist of coarse, beige-greenish, poorly sorted carbonate sand-silt with abundant organic macro-remains and fragments of lacustrine gastropods [A8] (Fig. 3). Several distinct white carbonate sand layers, characterized by high density, are intercalated within this silty-sandy unit. The sand is punctuated with hard, solid pieces of limestone, and it is interbedded by up to 5 mm thick, fining-upward, graded sand turbidites. The petrophysical analysis of this lithological unit revealed a trend of increasing density from *ca* 1·4 to 1·8 g cm^{-3} and magnetic susceptibility from *ca* 50 to 70×10^{-6} SI.

Basal Gravel Unit

Sediments of the BGU at the base of sites PI-3, PI-6 and PI-2 consist of solid, large limestone gravels (up to 4 cm) embedded in a poorly sorted, coarse, beige carbonate sand matrix. The gravels usually are angular, but in some cases are rounded. The sand contains fragments of terrestrial gastropod shells [E]. The petrophysical analysis of this lithological unit revealed high density (*ca* 1·9 g cm^{-3}) and intermediate to high magnetic susceptibility (*ca* 55×10^{-6} SI).

Mottled Unit (ca 85 to ? ka)

This unit, which only occurs in shallow-water site PI-7, intercalated between overlying Unit VI and underlying Unit IX, consists of a more than 30 m thick, sticky, light-bluish-grey to dark-yellowish-orange, fine-grained mud-silt sequence [F]. The mineralogy of this unit is composed mainly of calcite, montmorillonite and pyrite. The grey sediments of this sequence are often mottled with dark black, diffuse spots. The Mottled Unit is characterized by many cracks, which display a reddish hue, probably associated with sediment oxidation. This section has intermediate magnetic susceptibility, high density, low organic matter (mean *ca* 1%), and high calcium carbonate content (mean *ca* 15%).

Unit IX (? to 200 ka)

Unit IX, recovered only at sites PI-1 and PI-7, represents sediments deposited some time before a hiatus that ended *ca* 85 ka and at least 200 ka. This unit is characterized by alternations of two kinds of packages and is up to 10 m thick: (i) dark, brown-greenish, finely laminated (millimetre-scale) carbonate-clay mud [A7]; and (ii) bright beige, very homogenous carbonate mud [A6]. The darker, clay-rich packages are full of planktonic diatoms (*Aulacoseira* sp.), whereas the lighter, calcite-rich packages are dominated by benthonic diatoms (*Mastogloia* and *Denticula*). Thus, rhythmic alternations between darker and lighter packages suggest fluctuations between higher and lower lake levels, respectively. Sediments of Unit IX are often interbedded with dark, graded turbidites [A3], and they are composed of

many millimetre-scale to decimetre-scale deformation structures (Fig. 8). Such structures are expressed in the sediment record as: (i) millimetre-scale folded laminations; or (ii) large slump structures, which are visible as prominent deformations of thick turbidites (Fig. 8).

Basement (BSE)
At sites PI-7 and PI-1, material recovered below the sediments of Unit IX is interpreted as representing bedrock [G]. It consists of large, angular, white-beige limestone gravels in a coarse, sandy carbonate matrix.

Seismic stratigraphy

The initial seismic stratigraphy of Anselmetti *et al.* (2006) was modified and five major seismic sequences (T, G, P, R and B) and several sub-sequences that overlie the acoustic basement were identified (Figs 5 to 7; Table 5). Capital letters indicate the colour used to illustrate the seismic reflection that marks the underlying sequence boundary, i.e. T(urquoise), G(reen), P(ink), R(ed) and B(lue). Sub-sequences are indicated by numerals 1 to 5 or, in the case of the 'Maya-Clay', by 'T$_m$' (Fig. 10).

Core-to-seismic correlation

Core-to-seismic correlation is shown along an east–west seismic reflection profile, and along crossing north–south profiles (Figs 5 to 7). Lithological Unit I spans the Holocene and coincides with uppermost seismic sequence T (Fig. 6). The bulk of Unit I was deposited in a relatively short period between *ca* 1·0 and 3·0 ka, and is represented by the 'Maya-Clay' sub-unit (I$_m$) and in the seismic reflection data by sub-sequence T$_m$ (Fig. 10). The lithological boundary from Unit I (clay) to Unit II (gypsum) at *ca* 10·7 ka is expressed by a prominent increase in bulk density (from *ca* 1·4 to *ca* 1·7 g cm^{-3}) and a strong, high-amplitude reflection at seismic boundary T/G (Fig. 6). Sediments of Unit II (10 to 18 ka) consist of three gypsum sub-units (IIa, IIc and IIe) and two clay sub-units (IIb and IId). The top of each gypsum sub-unit corresponds to one of three stacked palaeoshorelines (PS) in the seismic record at 75 ms (PS-G1, 56 m), 85 ms (PS-G2, 64 m) and 90 ms (PS-G3, 68 m) (Figs 6 and 7). Clay-rich sediments of Unit III (18 to 23 ka) are characterized by low bulk densities and are represented seismically by low-amplitude reflections of seismic sequence P. The sedimentological

transition from Unit III (clay) to Unit IV (gypsum) at 23 ka is expressed by an increase in density from *ca* 1·5 to *ca* 1·9 g cm^{-3} in the core, which corresponds to a strong, high-amplitude reflection at the P/R sequence boundary. Sediments of Unit IV (23 to 39 ka), consisting of alternating gypsum sub-units (IVa, IVc, IVe and IVg) and clay sub-units (IVb, IVd and IVf), are marked by high-frequency variations in bulk density, and coincide approximately with continuous, high-amplitude reflections of sub-sequence R1. Lithological Unit V (39 to 49 ka) correlates with seismic sub-sequence R2. Some areas in sub-sequence R2 show transparent to chaotic seismic facies, indicating local mass movements that are also observed in lithological Unit V as deformed sediments, on metre to millimetre scales (Fig. 8). The clay-rich mud of Unit VI (49 to 58 ka) represents the upper part of sequence B. Banded, clay-rich and carbonate-rich lacustrine sediments of Unit VII (58 to 78 ka) correspond to the middle part of sequence B. The transition from Unit VIII (78 to 85 ka) to Unit VII at 78 ka corresponds to the lower part of sequence B and is expressed by an up-core decrease in density from *ca* 1·9 to *ca* 1·5 g cm^{-3} (Fig. 6). Sediments of MU (Site PI-7) and lithological Unit IX, that cover the time span from *ca* 85 to *ca* 200 ka in sites PI-1 and PI-7, could not be correlated with the seismic record, as the air-gun source was insufficient to penetrate to this sediment depth (Fig. 7). Consequently, recovery of these deposits was unexpected because they were not imaged by the seismic reflection survey.

DISCUSSION

Comparisons with the seismic model of Anselmetti *et al.* (2006)

The entire sediment record from Lake Petén Itzá was used to evaluate and refine the previous seismic stratigraphic work of Anselmetti *et al.* (2006). In general, the earlier study shows good agreement with the observations presented in this study (Fig. 6). Nonetheless, there are some significant differences between the findings of this study and the interpretations of Anselmetti *et al.* (2006).

1 Whereas Anselmetti *et al.* (2006) defined four seismic sequences (T, G, R and B), an additional major seismic sequence P was defined in this study. Sequence P spans the LGM, from 18 to

© 2010 The Authors. Journal compilation © 2010 International Association of Sedimentologists, *Sedimentology*, **57**, 1220–1245

Table 5. Seismic geometries and seismic facies of each seismic sequence in the sediment record of Lake Petén Itzá, described from the top (young sediments) to the bottom (old sediments).

Sequence T
Sequence T is composed of a thick (10 to 15 m) succession of acoustically stratified sediments characterized by highly continuous, low-amplitude reflections. Locally, internal reflections are characterized by higher amplitudes than those of surrounding reflections. Sequence T is separated from the underlying sequence G by a high-amplitude reflection, which is onlapped by the younger reflections of sequence T. Sequence T reaches a maximum thickness of *ca* 15 m in the deeper parts of the basin. On the high-resolution pinger seismic lines a mappable subunit (Tm) is recognized within sequence T. Subsequence Tm is characterized by slightly higher amplitude reflections than the rest of sequence T. The thickest part of subsequence Tm reaches values of more than 7 m, coincident with maximum water depth

Sequence G
Sequence G is thickest in the deeper parts of the basin, reaching a maximum thickness of *ca* 20 m. Reflections of sequence G are characterized by continuous reflections, similar to sequence T, but with higher amplitudes. On the slightly dipping southern part of the basin, the top of sequence G is characterized by a mound-like clear feature occurring at *ca* 56 m (75 ms) below modern water level. This feature can be observed throughout the entire Petén Itzá basin and is interpreted as a palaeoshoreline (Anselmetti *et al.*, 2006). Similar to this palaeoshoreline, two other buildups at *ca* 64 m (85 ms) and at *ca* 68 m (90 ms) below modern lake level are documented, representing two additional stacked palaeoshorelines. These three build-ups separate sequence G into three subsequences G1, G2 and G3

Sequence P
The depocentre of sequence P, where this unit reaches a maximal vertical thickness of 12 m, is coincident with maximum water depth (160 m). This sequence is characterized by continuous, low-amplitude reflections. The top of sequence P is defined by a normal-polarity high-amplitude reflection and the base is defined by an inverse-polarity high-amplitude reflection (compared to the normal-polarity lake floor reflection representing a downward increasing impedance). Sequence P constantly wedges out at a water depth of *ca* 85 ms two-way-travel (64 m below modern lake level). The bottom of this sequence is characterized by an onlap geometry onto the top of sequence R1

Sequence R
Sequence R is subdivided into an upper Subsequence R1 and a lower subsequence R2 using an inverse-polarity high-amplitude reflection. The reflections of both sequences R1 and R2 are generally higher amplitudes near the basin edges and get weaker with increasing water depth and distance from the basin margin. Some areas show transparent to chaotic seismic facies indicating local mass movements

Sequence B
The oldest seismic-stratigraphic sequence B reaches a maximum thickness of 50 to 60 m where it infills bedrock depressions. These topographic lows in the bedrock are onlapped by sequence B. In general, the seismic facies of sequence B is more chaotic compared to the overlying sequences, but occasionally sequence B is also characterized by seismically stratified reflections

23 ka. This sequence was added because Unit III ('LGM-Clay') stands out, not only with respect to its lithological signature, but because its seismic facies is characterized by very low reflection amplitudes that contrast sharply with overlying and underlying seismic sequences.

2 Sequence G, defined in Anselmetti *et al.* (2006) as containing two sub-sequences, was subdivided into three sub-sequences G1, G2 and G3. New evaluation revealed that the three-fold succession of gypsum sediments in Unit II (or sequence G) matches three seismically identified, stacked PS (Figs 6 and 7) that were not recognized before. The three PS, at −68 m, −64 m and −56 m, thus indicate a stepwise increase in palaeolake water levels after lowstands during the arid, last deglaciation phase (11 to 18 ka).

3 At sites PI-1 and PI-7, drilling penetrated significantly beyond predictions made using seismic reflection data, i.e. below the apparent 'acoustic basement'. This under-estimation was caused in part by high-impedance values of the BGU in contrast to the overlying units. Furthermore, large limestone clasts in the BGU scatter the acoustic signal, thereby inhibiting deeper acoustic penetration. Interpretation of the seismic reflection data accurately predicted the sub-surface depth down to the base of Unit VIII and BGU, which appeared as acoustic basement in the deeper-water sections. The occurrence of sediments in Unit IX, below the acoustic basement, which were undetected seismically, probably is limited to the deeper-water depocentres of the lake. In shallow-water areas in contrast, the

seismically mapped acoustic basement may well represent 'true' basement, as it is exposed nearby on the lake shores.

Lake level and sedimentation history of Lake Petén Itzá

Eleven lithological units (Units I to IX, MU and BGU) were defined in the stratigraphic record overlying the BSE of Lake Petén Itzá, and represent at least 11 distinct phases of the palaeo-environmental history of the lake. Stratigraphic correlation of these lithological unit boundaries (Fig. 3) and seismic reflections (Fig. 5) throughout the basin indicates that the lithology can be used as a reliable proxy for palaeolimnological and palaeoclimate inferences. Sedimentological results are interpreted and discussed with respect to past lake and environmental changes, from oldest to youngest deposits (Fig. 11).

The oldest lacustrine sediments of Lake Petén Itzá, which overlie the basement, are represented by lithological Unit IX in sites PI-1 and PI-7 and reach a basal age of *ca* 200 ka, corresponding to the transition from MIS 7 to MIS 6. This rather young age does not necessarily represent the age of the initial lake formation. Older sediments may have been eroded and redeposited in the deeper parts of the bedrock topography. Due to the low energy of the acoustic signal produced by the airgun source used in the seismic reflection survey, seismic energy did not penetrate to bedrock in these deeper areas; therefore, continuous mapping of the bedrock surface was not possible. In marginal areas of the lake, where the bedrock surface can be traced with seismic reflection data, the morphology suggests a half graben geometry, with a steep northern border fault and a gently dipping southern graben shoulder. Both appear to be enhanced by karstic dissolution processes, which contributed to lake basin formation (Anselmetti *et al.*, 2006). Observed sediment deformation and the slumping and sliding of entire sediment packages (Fig. 8) may be the result of ongoing tectonic activity. These features may also be a consequence of sediment 'overloading', produced by lake level changes that altered geotechnical properties and decreased slope stabilities, or alternatively as a consequence of distant seismic events. No evidence of faults (for example, with surface ruptures) was observed in the seismic reflection data. Thus, there is no direct evidence of ongoing tectonic activity in the sub-surface of Lake Petén Itzá.

Sandy to silty carbonates [A8], interbedded by numerous dark, clay-sand turbidites [A3] in unit IX, overlie the basement and indicate high run-off and detrital input from the watershed into the lake. This observation would imply relatively humid conditions during the initial transgression and lake-filling phase. Nevertheless, if the lake basin and catchment morphology were very different from that of today, perhaps as a consequence of tectono-karstic alterations, the hydrology of the system may also have differed. A hydrologically 'open' system would not have been as susceptible to evaporite formation as the lake is today. Hence, the rather uniform lithologies could have been produced in an open system that was relatively insensitive to E/P changes. The lack of major lithological changes in this unit, however, is remarkable, especially considering the large glacial–interglacial changes and variations in precessionally driven insolation that occurred during this period.

At shallow-water Site PI-7, Unit IX is overlain by MU, which is composed of a peculiar, >30 m thick succession of bluish to yellowish, carbonate-clay-pyrite mud [F] that lacks visible layering. The mottled bluish lithology is reminiscent of gleyed soil, which usually forms under low-oxygen, high soil-moisture conditions followed by flooding (Gambrell & Patrick, 1978; Reddy *et al.*, 1986). Sediments overlying Unit IX in deep-water areas (for example, sites PI-2, PI-3 and PI-6) are represented by the BGU. These BGU sediments represent a partially exposed beach gravel horizon formed during a low lake stand before 85 ka, when soil formation, represented by MU, was taking place at shallow water site PI-7. Because seismic information below the BGU horizon is lacking, it is not possible to determine whether only sites PI-1 and PI-7 contain a pre-85 ka section such as Unit IX, or whether Unit IX is restricted to narrow depressions in the tectono-karstic substrate of Lake Petén Itzá. A seismic reflection survey, using a stronger acoustic source, might provide the answer. Because Site PI-4, located near the greatest water depth of the modern lake, was not drilled to bedrock, it is also uncertain whether the BGU horizon develops into a conformable succession at greater water depth. In any case, this horizon represents a major lake level lowering around 90 ka, most probably caused by a significant increase in E/P. In this regard it is noteworthy that lake level lowstands (i.e. climate drying) around this time have also been inferred for low-latitude African lakes
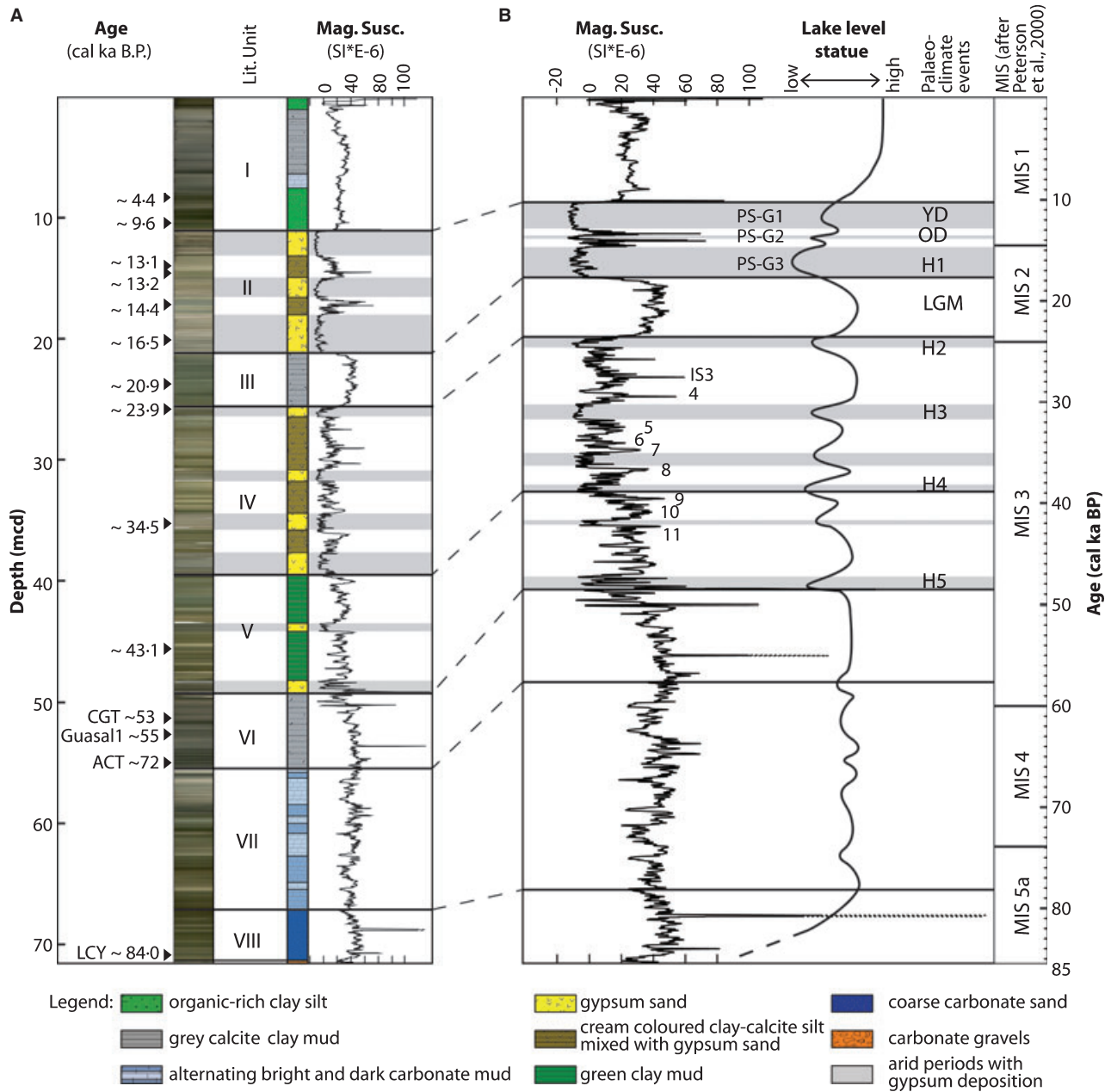
Fig. 11. (A) Compiled data from site PI-6 versus depth (mcd): Radiocarbon and tephra ages in cal ka BP at sample locations, composite photograph scan, lithological units, stratigraphic column and magnetic susceptibility. Gypsum deposits (marked by yellow colour and low magnetic susceptibility) are highlighted by grey shading and correlate with Heinrich Events 'H' that occur in the coldest stadials in Greenland (Bond *et al.*, 1992). 'YD', Younger Dryas; 'LGM', Last Glacial Maximum; 'OD', Older Dryas. (B) Compiled data from site PI-6 versus age in cal ka BP and Marine Isotope Stage (MIS, from Peterson *et al.*, 2000): magnetic susceptibility (SI × 10^{-6}) with Greenland interstadial (IS) events (Hodell *et al.*, 2008) and schematic lake level curve from Lake Petén Itzá based on the presented seismic, lithological and magnetic susceptibility data.

(for example, Lakes Malawi, Bosumtwi and Tanganyika; Scholz *et al.*, 2007).

After deposition of the BGU between 85 and 78 ka (*ca* MIS 5a), a rise in lake level and transgression are indicated by coarse carbonate sand with large gastropods in Unit VIII [A8].

This lithology represents a shallow, transgressional depositional environment with high energy during the flooding phase. Because site PI-7 was drilled in shallow water, it was flooded by this transgression at a later date, during deposition of Unit VI.

The sequence spanning *ca* 78 to *ca* 58 ka (*ca* MIS 4) includes shallower-water and deeper-water sediments (Unit VII) [A6, A7], representing alternating dry and humid climate conditions. Phases of lower lake level were not sufficiently low or persistent enough to reach $CaSO_4$ saturation, which is required to precipitate gypsum. Nonetheless, alternating lake levels are documented in the sediment record (Unit VII) by intercalated bright-beige carbonate [A6], and dark brown to greenish, carbonate-clay beds [A7]. The brighter carbonate-rich bands represent shallow-water conditions containing benthonic, shallow-water diatoms (*Mastogloia*, *Denticula*), whereas the darker clay beds represent deep-water conditions containing planktonic diatoms (*Aulacoseira* sp.).

The time between 58 and 49 ka (early MIS 3) was characterized by relatively humid conditions (i.e. high lake level) as indicated by the high detrital clay content [A1] Unit VI, suggesting high run-off and detrital input from the watershed during times of greater rainfall. Between 49 and 39 ka (mid-MIS 3), high lake level stands and humid conditions continued as indicated by high organic matter content in the detrital sediments of Unit V [A4], suggesting higher autochthonous organic matter production during a period of less saline conditions. This overall humid period was interrupted by two short, but pronounced lake level drops during dry events at *ca* 48 and *ca* 42 ka. During these two dry events, the volume of Lake Petén Itzá was reduced significantly and lake waters were more saline than today, causing the first episodes of authigenic gypsum precipitation [B].

The time between 39 and 23 ka (late MIS 3) was characterized by fluctuating high and low lake levels. In Unit IV, stage variations are documented by gypsum layers [B] during lowstands that alternate with cream-coloured, carbonate-clay silt [A5] deposits during highstands. Four lowstands, at *ca* 38·5, *ca* 35·5, *ca* 31 and *ca* 24 ka occur between three phases of higher lake level. The timing of clay-gypsum oscillations during the middle and later part of MIS 3 indicates that clay units correlate with warmer IS events documented in Greenland ice cores, whereas gypsum units are associated with cold stadials in the North Atlantic, especially those containing Heinrich Events H4, H3 and H2 (Bond *et al.*, 1992; Hodell *et al.*, 2008) (Fig. 11). Similarly, alternating clay-gypsum units during MIS 3 correlate closely with other circum-Caribbean palaeoclimate records, for instance, the marine Cariaco

Basin record off northern Venezuela (ODP Hole 1002C; Peterson *et al.*, 2000; Hodell *et al.*, 2008). These Dansgaard-Oeschger climate cycles (Dansgaard *et al.*, 1993) are also represented in the seismic data by high-amplitude reflections within sequence R1 (Fig. 6), which are produced by lithological differences between low-density clay and high-density gypsum sediments.

From 23 to 18 ka, i.e. during the LGM (Mix *et al.*, 2001) (early MIS 2), high lake level (i.e. humid climate) and enhanced erosion are indicated by several lines of evidence. Firstly, the sediment is dominated by montmorillonitic clays (Unit III). As montmorillonite is the principal weathering product of tropical soils in Petén (Cowgill & Hutchinson, 1966; Curtis *et al.*, 1998), it suggests a humid climate and pronounced erosion in the watershed. Secondly, the dark-coloured turbidites [A3] represent individual heavy precipitation events. Thirdly, high magnetic susceptibility values indicate high deposition of clastic material in the lake. Lastly, the base of sequence P onlaps onto underlying sequence R1 and there is a basinward-thickening wedge of seismic sequence P seen on seismic reflection data (Fig. 7), with the depocentre of this sequence coincident with the greatest water depths. These findings are consistent with enhanced detrital input, suggesting sediment focusing into deeper parts of the basin (i.e. high-density turbidites from underflows). These sedimentological characteristics all indicate humid climate during the LGM, which contradicts previous palaeoclimate results from Petén that proposed the lowlands of Central America were dry at that time (Leyden *et al.*, 1993, 1994). Previous inferences, however, were based on the poorly dated sequence from Lake Quexil. Climate mechanisms that may have produced a humid climate in Petén during the LGM are discussed in Hodell *et al.* (2008) and Bush *et al.* (2009).

During the last deglaciation from 18 to 11 ka (late MIS 2, early MIS 1), lake levels fluctuated between low and intermediate stands as indicated in Unit II by alternating gypsum [B] and cream-coloured, clay-carbonate units [A5]. The lithology suggests a generally arid Late Glacial. In the seismic record, effective moisture cycles are recognized by the increased frequency of high-amplitude reflections in seismic sequence G. Three dry events, i.e. lake level lowstands, are recorded by three gypsum units at *ca* 16·5, *ca* 14 and *ca* 11·5 ka, all of which have a palaeoshoreline in the lake margin areas (PS-G1-3, Figs 6, 7 and 11). The elevations of these shorelines

increase successively from 68 m (90 ms) to 64 m (85 ms) and finally to 56 m (75 ms) below the modern lake level (Figs 6, 7 and 11), showing a stepwise increase in the level of the lowstands during the Late Glacial.

About 11 ka, at the termination of the arid last glacial period in early MIS 1, the lake level was *ca* 56 m below the modern stage, as indicated by a palaeosol in shallow-water cores (Hillesheim *et al.*, 2005; Anselmetti *et al.*, 2006) and by autochthonous gypsum crystals in deep-water cores (Hillesheim *et al.*, 2005; Anselmetti *et al.*, 2006). At that time, the volume of Lake Petén Itzá was reduced to only about 13% of its present volume, the lake was moderately saline and waters were saturated with respect to gypsum (Hillesheim *et al.*, 2005). After this lowstand, lake levels rose, as documented in shallow-water cores by transgressive, gastropod-rich lacustrine sediments, which overlie a late Pleistocene palaeosol (Curtis *et al.*, 1998; Hillesheim *et al.*, 2005). In deep-water cores, the transition from arid late Pleistocene to moister Holocene conditions is marked by a shift from gypsum [B] to organic-rich, deeper-water, clay-rich sediments of Unit I [A4]. Onlapping bedding geometries in seismic sequence T clearly illustrate this lake transgression (Fig. 6). After this early Holocene rise, lake levels remained high except for minor phases of lowered levels, in particular between 4·5 and 3·0 ka (Mueller *et al.*, 2009) During the last 3 kyr, environmental conditions in Petén watersheds and sedimentology in the lakes have been controlled strongly by human activities (Deevey *et al.*, 1979; Binford *et al.*, 1987; Brenner, 1994; Rosenmeier *et al.*, 2002; Anselmetti *et al.*, 2007). For instance, forest clearance by the ancient Maya, which began about 3000 years ago, led to high erosion rates in Petén watersheds. This effect is expressed in the Lake Petén Itzá sediment record by the 'Maya-Clay' sub-unit (I_m) (Fig. 10). Following the demise of Classic Maya culture around 1·0 ka, rapid clay deposition was replaced by slower sedimentation of organic-rich clay and silt deposits, reflecting tropical forest recovery in the watershed and reduced supply of detrital material to the lake basin (Islebe *et al.*, 1996).

CONCLUSIONS

Lake Petén Itzá sediments are sensitive recorders of past environmental changes during the last 200 kyr. Seismic stratigraphy, together with sediment core analysis, enabled comprehensive reconstruction of past environmental changes in the region.

1 Radiocarbon dates and tephrochronology reveal that the oldest sediments of Lake Petén Itzá were deposited *ca* 200 ka (Marine Isotope Stage 7a). These samples were recovered from sections below the zone of deepest seismic imaging; accordingly deeper basins in the bedrock morphology may exist, and the age of the sampled sediments may under-estimate the age of tectono-karstic basin formation.

2 Eleven lithostratigraphic units (Units I to IX, Mottled Units and Basel Gravel Units) overlying the basement were defined in the Petén Itzá sediment record. These units represent at least 11 distinct phases of the palaeoenvironmental history of the lake. These lithostratigraphic units are traceable laterally throughout the Lake Petén Itzá basin. This observation justifies the use of the lithological succession as a regional palaeoenvironmental proxy, as suggested by previous studies (Hodell *et al.*, 2008).

3 The sediment succession in cores from the seven drill sites allowed testing and refinement of the seismic stratigraphy proposed prior to drilling. The predictions of stratigraphic boundaries, in general, were accurate. Seismic data penetration was not sufficient to image deep sediment in some sections. In two cases, reflections interpreted as acoustic basement were instead a gravel-bearing horizon and sediments were much thicker than anticipated.

4 Sediment deposited between *ca* 200 and 85 ka was encountered at only two sites, probably because of irregular basin morphology with narrow depressions in the tectono-karstic basement. These oldest sediments are characterized by lithologies that reflect deposition during an initial transgression, followed by clay and carbonate-rich sediments without major gypsum units, reflecting rather sustained humid conditions resulting in high run-off and high detrital constituents.

5 Before 85 ka, the sediment record is characterized by a gravel-bearing and sand-bearing unit that forms an unconformity indicative of a major lake level lowstand (i.e. dry climate). Dry climate around this time was also inferred by study of sediments from low-latitude African lakes.

6 During the last *ca* 50 kyr, lithological units are characterized by alternating clay and gypsum units. Gypsum units are associated with low lake levels (i.e. dry climate) and clay units with high lake levels (i.e. humid climate). Stacked palaeo-shorelines at −68 m, −64 m and −56 m coincide

with gypsum units that indicate a stepwise increase in water levels from the lowstands during the arid, last deglaciation, 18 to 11 ka.

7 The Holocene lacks gypsum deposits, and was thus characterized by relatively high lake levels and humid climate. Human impact during the Maya epoch (*ca* 3·0 to 1·0 ka) is reflected by rapid clay deposition.

REFERENCES

Anselmetti, F.S., Ariztegui, D., Hodell, D.A., Hillesheim, M.B., Brenner, M., Gilli, A., McKenzie, J.A. and **Mueller, A.D.** (2006) Late Quaternary climate-induced lake level variations in Lake Petén Itzá, Guatemala, inferred from seismic stratigraphic analysis. *Palaeogeogr. Palaeoclimatol. Palaeoecol.*, **230,** 52–69.

Anselmetti, F.S., Ariztegui, D., Brenner, M., Hodell, D.A. and **Rosenmeier, M.F.** (2007) Quantification of soil erosion rates related to ancient Maya deforestation. *Geology*, **35,** 915–918.

Beach, T., Dunning, N., Luzzader-Beach, S., Cook, D.E. and **Lohse, J.** (2006) Impacts of the ancient Maya on soils and soil erosion in the Central Maya lowlands. *Catena*, **65,** 166–178.

Binford, M.W., Brenner, M., Whitmore, T.J., Higuera-Gundy, A., Deevey, E.S. and **Leyden, B.** (1987) Ecosystems, paleoecology and human disturbance in subtropical and tropical America. *Quatern. Sci. Rev.*, **6,** 115–128.

Bond, G., Heinrich, H., Broecker, W., Labeyrie, L., McManus, J., Andrews, J., Huon, S., Jantschik, R., Clasen, S., Simet, C., Tedesco, K., Klas, M., Bonani, G. and **Ivy, S.** (1992) Evidence for massive discharges of icebergs into the North Atlantic Ocean during the last glacial period. *Nature*, **360,** 245–249.

Brenner, M. (1994) Lakes Salpeten and Quexil, Petén, Guatemala, Central America. In: *Global Geological Record of Lake Basins* (Eds E. Gierlowski-Kordesch and K. Kelts), Vol. 1, pp. 377–380. Cambridge University Press, Cambridge.

Brenner, M., Leyden, B.W. and **Binford, M.W.** (1990) Recent sedimentary histories of shallow lakes in the Guatemalan savannas. *J. Paleolimnol.*, **4,** 239–251.

Bush, M.B., Correa-Metrio, A., Hodell, D.A., Brenner, M., Anselmetti, F.S., Ariztegui, D., Mueller, A.D., Curtis, J.H., Grzesik, D., Burton, C. and **Gilli, A.** (2009) Re-evaluation of climate change in lowland Central America during the Last Glacial Maximum using new sediment cores from Lake Petén Itzá, Guatemala. In: *Past Climate Variability in South America and Surrounding Regions* (Eds F. Vimeux, F. Sylvestre and M. Khodri), pp. 113–128. Springer, Netherlands.

Cowgill, U.M. and **Hutchinson, E.G.** (1966) La Aguada de Santa Ana Vieja: the history of a pond in Guatemala. *Arch. Hydrobiol.*, **62,** 335–372.

Cowgill, U.M., Hutchinson, G.E., Racek, A.A., Goulden, C.E., Patrick, R. and **Tsukada, M.** (1966) The history of Laguna de Petenxil, a small lake in northern Guatemala. *Mem. Connecticut Acad. Arts Sci.*, **17,** 1–126.

Curtis, J.H., Brenner, M., Hodell, D.A., Balser, R.A., Islebe, G.A. and **Hooghiemstra, H.** (1998) A multi-proxy study of Holocene environmental change in the Maya Lowlands of Petén, Guatemala. *J. Paleolimnol.* **19,** 139–159.

Dansgaard, W., Johnsen, S.J., Clausen, H.B., Dahl-Jensen, D., Gundestrup, N.S., Hammer, C.U., Hvidberg, C.S., Steffensen, J.P., Sveinbørnsdottir, A.E., Jouzel, J. and **Bond, G.** (1993) Evidence for general instability of past climate from a 250-kyr icecore record. *Nature*, **364,** 218–220.

Deevey, E.S., Gross, M.S., Hutchinson, G.E. and Kraybill, H.L. (1954) The natural ^{14}C contents of materials from hard-water lakes. *Proc. Natl Acad. Sci. USA*, **40**, 285–288.

Deevey, E.S., Rice, D.S., Rice, P.M., Vaughan, H.H., Brenner, M. and Flannery, M.S. (1979) Mayan urbanism: impact on a tropical karst environment. *Science*, **206**, 298–306.

Deevey, E.S., Brenner, M. and Binford, M.W. (1983) Paleolimnology of the Peten Lake District, Guatemala, III. Late Pleistocene and Gamblian environments of the Maya area. *Hydrobiologia*, **103**, 211–216.

Fairbanks, R.G., Mortlock, R.A., Chiu, T.-C., Cao, L., Kaplan, A., Guilderson, T.P., Fairbanks, T.W. and Bloom, A.L. (2005) Marine radiocarbon calibration curve spanning 10,000 to 50,000 years B.P. based on paired 230Th/234U/238U and ^{14}C dates on Pristine Corals. *Quatern. Sci. Rev.*, **24**, 1781–1796.

Gambrell, R.P. and Patrick, W.H. (1978) Chemical and microbiological properties of anaerobic soils and sediments. In: *Plant Life in Anaerobic Environments* (Eds D.D. Hook and R.M.M. Crawford), pp. 375–423. Ann Arbor Science, Ann Arbor, MI.

Harders, R., Brückmann, W., Feeser, V., Kutterolf, S., Hensen, C. and Moerz, T. (2007) Are ash layers the controlling factor on translational sliding? *Geophys. Res. Abstracts*, **9**, 07917. SRef-ID: 1607-7962/gra/EGU2007-A-07917.

Haug, G.H., Hughen, K.A., Sigman, D.M., Peterson, L.C. and Röhl, U. (2001) Southward migration of the intertropical convergence zone through the Holocene. *Science*, **293**, 1304–1308.

Hillesheim, M.B., Hodell, D.A., Leyden, B.W., Brenner, M., Curtis, J.H., Anselmetti, F.S., Ariztegui, D., Buck, D.G., Guilderson, T.P., Rosenmeier, M.F. and Schnurrenberger, D.W. (2005) Climate change in lowland Central America during the late deglacial and early Holocene. *J. Quatern. Sci.*, **20**, 363–376.

Hodell, D.A., Anselmetti, F., Brenner, M., Ariztegi, D. and PISDP Scientific Party (2006) The Lake Petén Itzá Scientific Drilling Project. *Sci. Drilling*, **3**, 25–29.

Hodell, D.A., Anselmetti, F., Ariztegui, D., Brenner, M., Bush, M.B., Correa-Metrio, A., Curtis, J.H., Escobar, J., Gilli, A., Grzesik, D.A., Guilderson, T.P., Kutterolf, S. and Mueller, A.D. (2008) An 85-ka record of climate change in lowland Central America. *Quatern. Sci. Rev.*, **27**, 1152–1165.

Islebe, G.A., Hooghiemstra, H., Brenner, M., Curtis, J.H. and Hodell, D.A. (1996) A Holocene vegetation history from lowland Guatemala. *Holocene*, **6**, 265–271.

Kutterolf, S., Schacht, U., Wehrmann, H., Freundt, A. and Mörz, T. (2007) Onshore to offshore tephrostratigraphy and marine ash layer diagenesis in Central America. In: *Geology, Resources and Hazards* (Eds J. Buntschuh and G.E. Alvarado), Taylor & Francis/Balkema, London. ISBN 978-0-415-41648-1: 395-423.

Kutterolf, S., Freundt, A., Peréz, W., Mörz, T., Schacht, U., Wehrmann, H. and Schmincke, H.U. (2008a) Pacific offshore record of plinian arc volcanism in Central America: 1. Along-arc correlations. *Geochem. Geophys. Geosyst.*, **9**, Q02S01. doi: 10.1029/2007GC001631.

Kutterolf, S., Freundt, A., Schacht, U., Bürk, D., Harders, R., Mörz, T. and Peréz, W. (2008b). Pacific offshore record of plinian arc volcanism in Central America: 3. Application to forearc geology. *Geochem. Geophys. Geosyst.*, **9**, Q02S03. doi: 10.1029/2007GC001826.

Leyden, B.W. (1984) Guatemalan forest synthesis after Pleistocene aridity. *Proc. Natl Acad. Sci. USA*, **81**, 4856–4859.

Leyden, B.W. (1987) Man and climate in the Maya lowlands. *Quatern. Res.*, **28**, 407–414.

Leyden, B.W., Brenner, M., Hodell, D.A. and Curtis, J.H. (1993) Late Pleistocene climate in the Central American lowlands. In: *Climate Change in Continental Isotopic Records. Am. Geophys. Union, Geophys. Monogr.*, **78**, 165–178.

Leyden, B.W., Brenner, M., Hodell, D.A. and Curtis, J.H. (1994) Orbital and internal forcing of climate on the Yucatan Peninsula for the past ca. 36 ka. *Palaeogeogr. Palaeoclimatol. Palaeoecol.*, **109**, 193–210.

Mix, A., Bard, E. and Schneider, R. (2001) Environmental processes of the ice age: land, oceans, glaciers (EPILOG). *Quatern. Sci. Rev.*, **20**, 627–657.

Mueller, A.D., Islebe, G.A., Hillesheim, M.B., Grzesik, D.A., Anselmetti, F.S., Ariztegui, D., Brenner, M., Curtis, J., Hodell, D.A. and Venz, K.A. (2009) Climate drying and associated forest decline in the lowlands of Northern Guatemala during the Late Holocene. *Quatern. Res.*, **71**, 133–141.

Peterson, L.C., Haug, G.H., Hughen, K.A. and Röhl, U. (2000) Rapid changes in the hydrologic cycle of the tropical Atlantic during the Last Glacial. *Science*, **290**, 1947–1951.

Reddy, K.R., Feijtel, T.C. and Patrick, W.H. (1986) Effect of soil redox conditions on microbial oxidation of organic matter. In: *The Role of Organic Matter in Modern Agriculture* (Eds Y. Chen and Y. Avnimelech), pp. 117–156. Nijhoff, Dordrecht.

Rice, D.S., Rice, P.M. and Deevey, E.S. (1985) Paradise lost: classic Maya impact on a lacustrine environment. In: *Prehistoric Lowland Maya Environment and Subsistence Economy, Papers of the Peabody Museum of Archaeology and Ethnology* (Ed. M.D. Pohl), Vol. 77, pp. 91–105. Harvard University Press, Cambridge.

Rose, W.I., Conway, F.M., Pullinger, C.R., Deino, A. and McIntosh, W.C. (1999) An improved age framework for late Quaternary silicic eruptions in northern Central America. *Bull. Volcanol.*, **61**, 106–120.

Rosenmeier, M.F., Hodell, D.A., Brenner, M., Curtis, J.H. and Guilderson, T.P. (2002) A 4000-year lacustrine record of environmental change in the southern Maya lowlands, Petén, Guatemala. *Quatern. Res.*, **57**, 183–190.

Schnurrenberger, D., Russell, J. and Kelts, K. (2003) Classification of lacustrine sediments based on sedimentary components. *J. Paleolimnol.*, **29**, 141–154.

Scholz, C.A., Johnson, T.C., Cohen, A.S., King, J.W., Peck, J.A., Overpeck, J.T., Talbot, M.R., Brown, E.T., Kalindekafe, L., Amoako, P.Y.O., Lyons, R.P., Shanahan, T.M., Castañeda, I.S., Heil, C.W., Forman, S.L., McHargue, L.R., Beuning, K.R., Gomez, J. and Pierson, J. (2007) East African megadroughts between 135 and 75 thousand years ago and bearing on early-modern human origins. *Proc. Natl Acad. Sci. USA*, **104**, 16416–16421.

Stuiver, M. and Polach, H.A. (1977) Discussion: reporting of ^{14}C data. *Radiocarbon*, **19**, 355–363.

Ufer, K., Stanjek, H., Roth, G., Dohrmann, R., Kleeberg, R. and Kaufhold, S. (2008) Quantitative phase analysis of bentonites with the Rietveld method. *Clay Clay Mineral.*, **56**, 272–282.

Vail, P.R., Mitchum, R.M. and Thompson, S. (1977) Cycles of relative changes of sea level. In: *Seismic Stratigraphy – Applications to Hydrocarbon Exploration* (Ed. C.E. Payton), *AAPG Mem.*, **26**, 83–97.

Valero Garcés, B.L. and Kelts, K. (1995) A sedimentary facies model for perennial and meromictic saline lakes: Holocene

Medicine Lake Basin, South Dakota, USA. *J. Paleolimnol.*, **14**, 123–149.

Vaughan, H.H., Deevey, E.S. and **Garrett-Jones, S.E.** (1985) Pollen stratigraphy of two cores from the Petén Lake District. In: *Prehistoric Lowland Maya Environment and Subsistence Economy. Papers of the Peabody Museum of Archaeology and Ethnology* (Ed. M.D. Pohl), Vol. 77, pp. 73–89. Harvard University Press, Cambridge.

Vinson, G.L. (1962) Upper Cretaceous and Tertiary stratigraphy of Guatemala. *AAPG Bull.*, **46,** 425–456.

Young, R.A. (2002) The Rietveld method. In: *IUCr Monographs on Crystallography* (Ed. R.A. Young), Vol. 5. Oxford University Press, Oxford.